University of California

Santa Barbara

Potential for Stable Minor Sulfur Isotope Tracer to Measure Microbial Sulfur Reduction Rate and Fractionation Values Simultaneously

A thesis submitted in partial satisfaction of the

requirements for the degree Master's of Science

in Earth Science

by

Katherine Grace O'Malley

Committee in Charge:

Professor Morgan Raven

Professor Elizabeth Wilbanks

Professor Alexander Simms

December 2022

The thesis of Katherine G. O'Malley is approved.

Professor Alexander Simms

Professor Elizabeth Wilbanks

Professor Morgan Raven, Committee Chair

September 2022

Acknowledgements

Thank you to Morgan Raven, Tina Treude, Dave Valentine, and the NSF who made the NSF's AT42-19 research cruise possible. Special thank you to Braulio Castillo, Fox Bravo, and Lizzy Wilbanks for assisting with microbiology portions associated with the pure culture incubations. De'Marcus Robinson and David J. Yousavich who conducted the $^{35}S\text{-}SO_4^{2-}$ tracer incubations and Molly O'Beirne who was responsible for the $^{33}S\text{-}SO_4^{2-}$. Anna Schartman for her work on organizational and preservation of the ^{33}S core before COVID-19 closings.

Table of Contents

Figures

Tables

Equations

1	SO_4^{2-} (extracellular) ⇄ SO_4^{2-} (intracellular) ⇄ APS ⇄ SO_3^{2-} → H_2S	1
2a-c	$\delta^{33}S = [((^{33}S_{sample} + {}^{33}S_{label}) / (^{32}S_{sample} + {}^{32}S_{label})) / (^{33}S_{VCDT} / {}^{32}S_{VCDT}) - 1] * 1000$ Eq. 2a	3
	$\delta^{34}S = [((^{34}S_{sample} + {}^{34}S_{label}) / (^{32}S_{sample} + {}^{32}S_{label})) / (^{34}S_{VCDT} / {}^{32}S_{VCDT}) - 1] * 1000$ Eq. 2b	3
	$\delta^{36}S = [((^{36}S_{sample} + {}^{36}S_{label}) / (^{32}S_{sample} + {}^{32}S_{label})) / (^{36}S_{VCDT} / {}^{32}S_{VCDT}) - 1] * 1000$ Eq. 2c	3
3	$\Delta_{A\text{-}B}{}^{3x}S = \delta^{3x}S_A - \delta^{3x}S_B \cong \varepsilon_{A-B}$	3
4	$\varepsilon_{MSR} \cong \delta^{34}S\text{-}SO_4^{2-} - \delta^{34}S\text{-}H_2S$	3
5	Total $\delta^{33}S$ = Amount of H_2S new * $\delta^{33}S\text{-}H_2S_{new}$ + Amount of H_2S old * $\delta^{33}S\text{-}H_2S_{old}$	5
6	$^{33}S_{label}$ (µmol) = 0.98 * Vol_{label} * $[SO_4]_{label}$	9
7	$^{3x}S_{sample}$ (µmol) = $^{total}S_{sample}$ (µmol) * $(^{3x}S/^{32}S)_{sample}$ * $(^{32}S/^{tot}S)_{sample}$	9
8	$(^{32}S/^{tot}S)_{sample} = {}^{32}S_{sample} / [{}^{32}S_{sample} + {}^{33}S_{sample} + {}^{34}S_{sample} + {}^{36}S_{sample}]...$ $= 1 / (1 + (^{33}S/^{32}S)_{sample} + (^{34}S/^{32}S)_{sample} + (^{36}S/^{32}S)_{sample})$	10
9a-b	$^{34}\alpha = 1 + \varepsilon_{MSR}/1000$ Eq. 9a	10
	$^{33}\alpha = (^{34}\alpha - 1)^{0.515} + 1$ Eq. 9b	10
10	$\Delta^{33}S = \delta^{33}S_{H2S\ Final} - \delta^{33}S_{H2S\ Intial}$	10
11	Growth Rate, $\mu = (\ln [OD_2/OD_1]) / (T_2\text{-}T_1)$	20
12	Doubling Time = $\ln(2)/\mu$	20
13	Sulfate Turnover (%) = ($^{3x}SO_4^{2-}{}_{INTIAL}$ - $^{3x}SO_4^{2-}{}_{FINAL}$) / $^{3x}SO_4^{2-}{}_{INTIAL}$ * 100	26
14	Percent Recovery (%) = ($^{3x}SO_4^{2-}{}_{FINAL}$ + $^{3x}H_2S_{TOTAL}$) / $^{3x}SO_4^{2-}{}_{INTIAL}$ * 100	26
15	SRR = (amount of H_2S)/ (volume * time of incubation)	26
16	$\mathrm{csSRR} = \frac{SO_{4(2)}^{2-} - SO_{4(1)}^{2-}}{\frac{(cn_{(1)}+cn_{(2)})}{2} \cdot (T_{(2)} - T_{(1)})}$	27

Abstract

Microbial sulfate reduction (MSR) is the predominant pathway of organic matter (OM) degradation for half of all microbial cells in the ocean (Jorgensen 2019). However, measuring the rate and magnitude of MSR using well established radiotracer $^{35}S\text{-}SO_4^{2-}$ is limited logistically in the field by regulations on radioactive substances. This study lays the framework for the use of novel stable minor isotope ^{33}S labeled sulfate for *in situ* measurements of MSR and fractionations. The first stage of this study compares sulfate reduction rates of $^{33}SO_4^{2-}$ to those of $^{35}SO_4^{2-}$ by pure culture *Desulfovibrio vulgaris Hildenborough* (DvH) in parallel bottle incubations. The second half of this study focuses on parallel incubations of $^{33}SO_4^{2-}$ and $^{3}SO_4^{2-}$ in sediment cores from the sub-oxic Santa Barbara Basin (SBB) to examine SRR and model sulfur isotope compositions of newly formed sulfides at the surface where microbial activity and pyrite formation are most active (Reimers *et al.*, 1996; Raven *et al.*, 2016, Abdulla *et al.* 2020). The conclusions of these two studies pave the way for the eventual use of $^{33}SO_4^{2-}$ for *in situ* experiments where MSR is occurring rapidly and in large magnitudes.

Chapter 1. Introduction

Sulfate (SO_4^{2-}) is reduced to sulfide (H_2S) via microbial sulfate reduction (MSR) (Eq. 1) which can react with iron to form iron monosulfide (FeS) then pyrite (FeS_2) (Jørgensen *et al.*,1979) (Figure 1.1). Each transformation the sulfur atoms undergo within the cell presents an opportunity for the lighter sulfur isotopes (^{32}S) to be preferentially selected over the sulfur heavier isotopes (^{33}S, ^{34}S, ^{36}S). The resultant offset in the isotopic compositions of the product (sulfide) versus reactant (sulfate) is referred to as fractionation value.

$$SO_4^{2-}\ (\text{extracellular}) \rightleftarrows SO_4^{2-}\ (\text{intracellular}) \rightleftarrows APS \rightleftarrows SO_3^{2-} \rightarrow H_2S \qquad \text{Eq. 1}$$

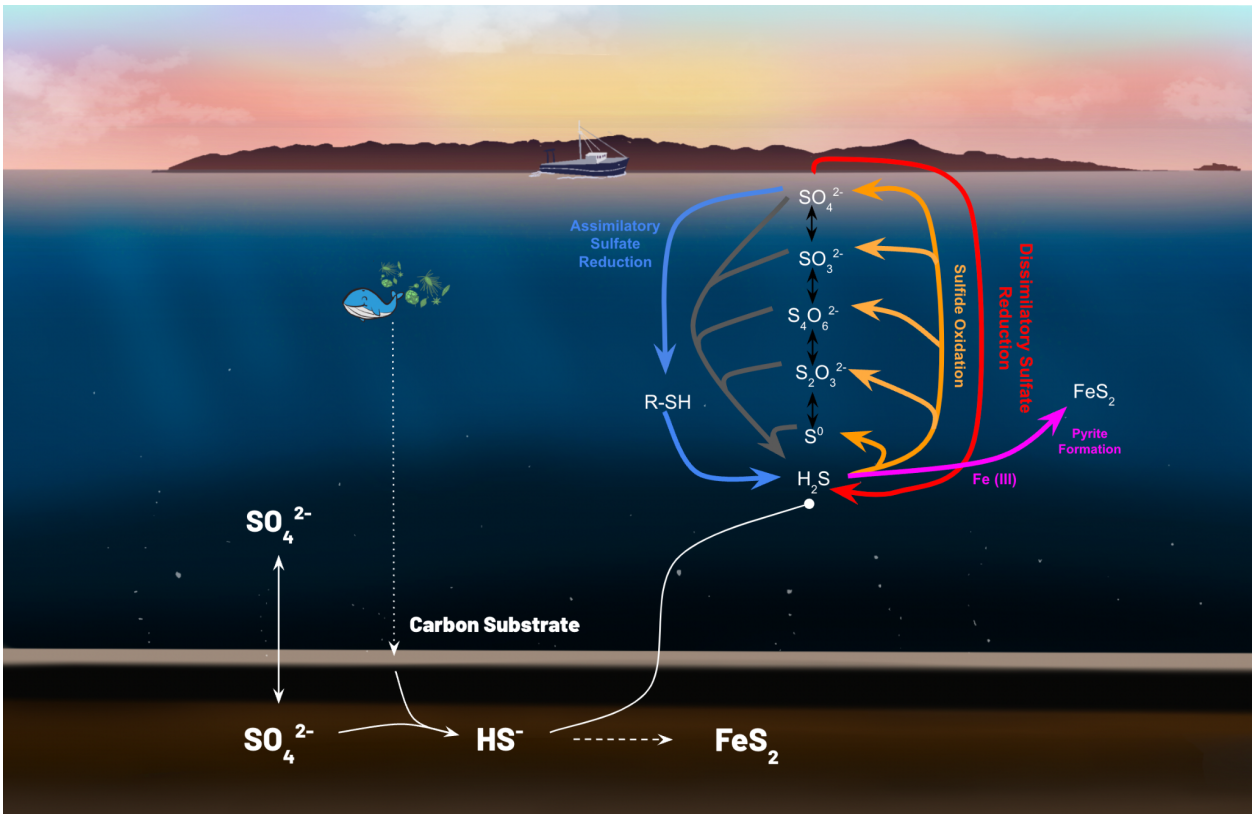

Figure 1.1 Sulfur Cycle Overview in SBB. Representation of sulfur species during sedimentary sulfur cycle in Santa Barbara Basin, California. Redrawn from Canfield 2001 and Jorgensen 1978.

The most abundant sulfur isotope, ^{32}S, accounts for 95% of all sulfur isotopes on earth. There are four minor isotopes which make up the remaining 5%: ^{33}S, ^{34}S, and ^{36}S, abundances are listed in Table 1.1. As MSR proceeds, we observe an enrichment of ^{32}S in sulfide and an enrichment of ^{34}S in the remaining sulfate in pore water. The resultant isotope offset is quantified as a fractionation. The extent of fractionation during MSR depends on a complex mixture of conditions dependent on enzymatic efficiencies, type and amount of electron donors, availability of sulfate, temperature, and pH. The magnitude of a fractionation can also dramatically increase when there is reversibility along the sulfur reduction pathway.

Table 1.1. Natural Abundances of Sulfur Isotopes from isotope standard Vienna-Canyon Diablo Troilite (VCDT) meteorite.

Isotope	Abundance in Decreasing Order
^{32}S	95.02%
^{34}S	4.22%
^{33}S	0.760%
^{36}S	0.0136%
^{35}S	Radioactive, $t_{1/2}$ = 87.5 days

Modern fractionations on Earth, with few exceptions, are mass-dependent thus, mass ratios of sulfur isotopes are a proxy for sulfate evolution with time (Canfield and Raiswell, 1999). Understanding the equations for natural abundance isotopic profiles is essential in evaluating how larger mixing and fractionation processes behave. The $\delta^{3x}S$ equation (Eq. 2a-c) is a ratio of isotopic ratios which defines the amount of the two minor isotopes present in a sample relative to a standard in linear space. MSR rates using ^{33}S-sulfide are made by the comparison of $^{33/32}S$ ratios in the sulfate phase versus the $^{33/32}S$ ratios of all total reduced inorganic sulfur phases.

The mass ratios are defined for specific to each minor isotope using Eq. 2a-c for $\delta^{33}S$, $\delta^{34}S$, and $\delta^{36}S$. All VCDT constants are listed in Table 1.2.

$$\delta^{33}S = [(({}^{33}S_{sample} + {}^{33}S_{label}) / ({}^{32}S_{sample} + {}^{32}S_{label})) / ({}^{33}S_{VCDT} / {}^{32}S_{VCDT}) - 1] * 1000 \quad \text{Eq. 2a}$$

$$\delta^{34}S = [(({}^{34}S_{sample} + {}^{34}S_{label}) / ({}^{32}S_{sample} + {}^{32}S_{label})) / ({}^{34}S_{VCDT} / {}^{32}S_{VCDT}) - 1] * 1000 \quad \text{Eq. 2b}$$

$$\delta^{36}S = [(({}^{36}S_{sample} + {}^{36}S_{label}) / ({}^{32}S_{sample} + {}^{32}S_{label})) / ({}^{36}S_{VCDT} / {}^{32}S_{VCDT}) - 1] * 1000 \quad \text{Eq. 2c}$$

Table 1.2. Constants Used for ^{33}S Tracer Calculations, Values Retrieved from Johnston (2011), λ constant for $^{33}\lambda$ a H_2S-SO_4 speciation within a temperature range of 0-110ºC.

Sulfur Isotope	VCDT Abundance	λ
32	0.9495	
34	0.0425	
33	0.0076	0.515
36	2.00E-04	1.91

When fractionations between two compounds of interest can be defined as the isotope difference, $\Delta^{3x}S$ which is defined in Eq. 3.

$$\Delta_{A\text{-}B}{}^{3x}S = \delta^{3x}S_A - \delta^{3x}S_B \cong \varepsilon_{A-B} \quad \text{Eq. 3}$$

Quantifying $\delta^{3x}S$ and $\Delta^{3x}S$ is an important tool in understanding how sulfur isotope compositions change through a series of biotic and abiotic transformations. Equations 4a and 4b assume that even in diverse environments the $\Delta^{33}S$ values of the MSR-derived sulfide pool are not sensitive to ε_{msr}. A comparison of the isotope composition of the product $\delta^{34}S$-H_2S, and the reactant, $\delta^{34}S$-SO_4^{2-} are represented by ε_{MSR} (Eq. 4).

$$\varepsilon_{MSR} \cong \delta^{34}S\text{-}SO_4^{2-} - \delta^{34}S\text{-}H_2S \quad \text{Eq. 4}$$

1.0 Epsilon ε_{MSR}

Epsilon ε_{MSR} accounts for the fractionation values produced as a direct result of MSR (eq. 4). The largest observed fractionations between sulfate and sulfide in the environment occur through microbial sulfate reduction. When sulfides react with available iron in the environment, ε_{MSR} values are captured in sedimentary pyrite which is preserved in the geological record. In palaeoceanographic studies, sulfur isotope compositions of pyrite are used as a proxy for MSR (Fike *et al.,* 2015; Pasquier *et al.,* 2017; Bertran *et al.* 2018, Liu *et al.,* 2020). Table 1.3 shows the range of epsilon values for each type of terrestrial and marine environment that hosts sulfate-reducers.

Table 1.3 Composition of various environments and observed $^{34}\varepsilon$ (‰).

		Location	$^{34}\varepsilon$ (‰)	Reference(s)
Terrestrial	Meromictic Lake	Heart Lake	0	Fry *et al.* (1995)
		Lake Mogil'noe	56-62	Ivanov *et al*. (2001)
	Holomictic Lake	Dart Lake, NY	3	Fry *et al*. (1995)
		Crystal Lake, NY	9	Fry *et al.* (1995)
		Lake Ontario	30	Demeters *et al.* (2001)
	Wetland	New Jersey Pinelands (swamp)	27	Mandernack *et al. (*2000)
		Everglades (swamp)	39-51	Price & Casagrande (1991)
	Groundwater	Bahamian blue holes	47-49	Bottrell *et al* (1991)
		Lincolnshire Aquifer	30-60	Bottrell (2000)
Marine	Continental	Baltic Sea	14-33	Demeters *et al.* (2001)

Shelf	Aarhus Bay	52-61	Johnston *et al. (*2008)
Coastal	Orinoco Delta (river delta)	8-15	Thode *et al.* (1960)
	Saint Lucia, Lesser Antilles	42-54	Ku *et al*. (2008)
Euxinic Basin	Baltic Sea	24-46	Demeters *et al.* (2001)
	Black Sea	43-66	Lyons (1997), Sweeney & Kaplan (1980), Fry *et al.* (1991), Johnston *et al.* (2008)
	Cariaco Basin	50-65	Fry *et al.* (1991), Werne et al., (2003), Li et al. (2010)
Deep Ocean	Santa Barbara Basin	0 to 48	Brüchert *et al.*, (1995), Kaplan *et al*. (1963), Raven *et al. (*2016)
	Santa Barbara Basin	**35-71**	Current Study
	Long Basin, California	68	Kaplan *et al* (1983)
	Peru Margin	27-55	Mossmann *et al.* (1991)
	Santa Catalina Basin	33-55	Kaplan *et al*. (1963)
	Santa Monica Basin	7-36	Kaplan *et al.* (1963)
	San Diego Trough	16-54	Kaplan *et al*. (1963)

The range of previously observed ε_{msr} values for deep ocean settings are a broad range from ε_{msr} =0 to 68‰ (Brüchert *et al.*, 1995, Kaplan *et al*. 1963, Raven *et al.* 2016, Mossmann *et al.* 1991) (Table 3.3). This broad range is a result of a mixture of sulfur reducing species and different types of substrates which fluctuate in between seasonal mixing events creating large fractionation deficits as a result of sustained nutrient deficiencies. Opposingly, small $^{34}\varepsilon$ values can be observed in times of substrate surplus following upwelling events (Brüchert *et al.*, 1995, Sim *et al.* 2011).

Over the course of several generations, $^{34}\varepsilon$ values may also gradually diminish as natural selection favors individual species with higher growth rates (Pellerin *et al.,* 2015). All factors considered create a broad range of observe ε_{msr} in deep marine sediments.

The largest fractionations expressed during MSR are often a function of the expressed equilibrium fractionation (Wing and Halevy, 2014). The composition of the organic matter varies locally, and the structural availability of the substrate directly impacts the anaerobic food chain (Abdulla *et al.* 2020). In marine sediments, large fractionations are associated with the slow degradation of recalcitrant organic substrates in the seabed (Leavitt *et al.*, 2013; Pellerin *et al.,* 2015). This occurs when there is not enough energy available for the metabolism to only follow the forward reaction pathway resulting in low rates of csrrR. When both forward and backward reactions occur, selectivity of the two isotopes becomes more extreme creating fractionations between sulfate and sulfide that approach thermodynamic equilibrium (Farquhar *et al.*, 2003). This may explain why ε_{MSR} values in natural populations in marine sediments appear to exceed the thermodynamic maximum at 71‰ (Sim *et al.* 2011) and atypically have a much wider range of csrrR than lab cultures (Figure 1.5). Quantifying sulfate reduction rates in the sediment as a function of $^{34}\varepsilon$ informs our interpretation of the availability of bioavailable carbon (Jorgensen *et al.* 2019).

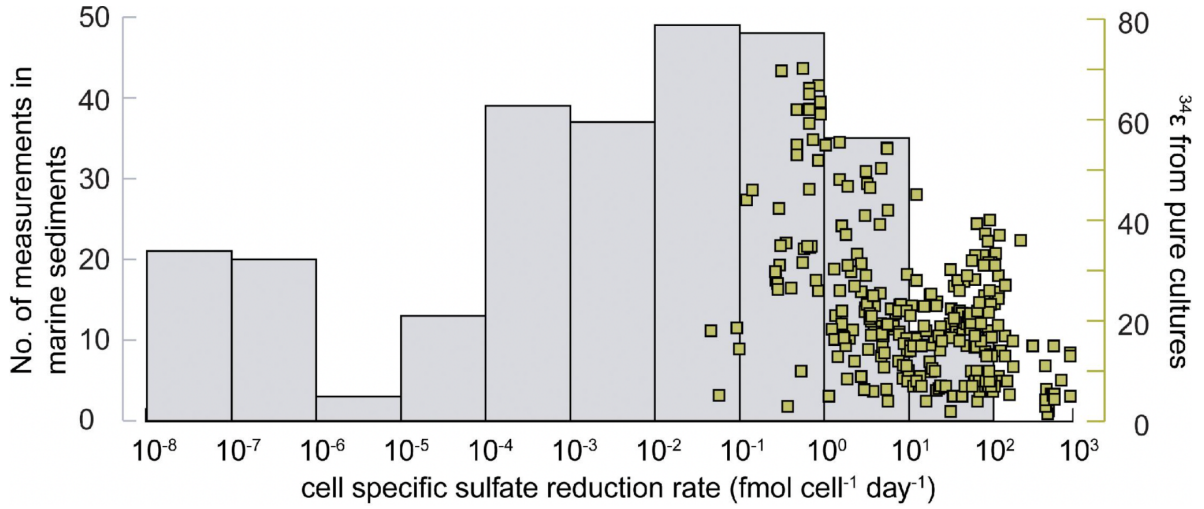

Figure 1.2 Frequency distribution of mean cell-specific sulfate reduction rates (csrrR). Gray bars (left axis) indicate the number of measurements in different csrrR-intervals in marine sediments. Green squares (right axis) plot distribution of csrrR in laboratory cultures. Figure and data compiled by Jorgensen (2019).

Our interpretation of the past relies closely on our understanding of the processes observed in modern sediments. While sulfur isotopic composition ($\delta^{34}S$) of sedimentary pyrite can inform us about large-scale chemical evolutions in paleoenvironments, $\delta^{34}S$ records are a result of localized microbial, depositional and post depositional processes (Fike *et al.,* 2015; Pasquier *et al.,* 2017; Liu *et al.,* 2020; Liu *et al.,* 2021). The sum of these conditions collectively impacts isotopic signatures. However, pore water sulfide signatures do not always match up with sedimentary pyrites. Physical isotope exchanges of individual atoms of sulfur move rapidly between the sulfide, polysulfide, elemental sulfur and iron sulfide (Figure 1.1) through a series of rapidly occurring biogeochemical processes which can be functionally impossible to detect and quantify.

Cryptic cycling is a term used in biogeochemistry to classify underlying chemical processes that are not detected by the porewater chemistry or reactive transport modeling (Jørgensen et al., 2019). Cryptic cycling is thought to account for the difference between gross and

net processes, such as the discrepancies between total SRR and the portion of accumulated sulfides lost to reoxidation. These gaps in chemistry for net processes which produce sulfides over the course of hours impact our interpretation of the sulfur isotope signatures preserved in pyrites and the environments they formed hundreds to thousands of years ago. The ultimate goal of this research is to develop the framework of a minor isotope labeled sulfate, $^{33}S\text{-}SO_4^{2-}$, to simultaneously quantify the rates of MSR and ε_{MSR} jointly. This would provide a tool to constrain cryptic rates of sulfur reduction at sites where MSR and oxidation are rapidly occurring.

1.1 Mathematical Theory Behind $^{33}SO_4^{2-}$ Tracer

Minor stable isotope, ^{33}S, is in a unique position as it makes up only 0.760% of the sulfate present in ocean water (Canfield 2001). This property makes ^{33}S a prime candidate as an isotopic label as any uptick in ^{33}S concentrations is easily spotted from natural abundance isotope compositions. Knowing the $\delta^{33}S$ of the label ($\delta^{33}S\text{-}H_2S_{label}$) and the initial sulfide pool ($\delta^{33}S\text{-}H_2S_{old}$), a mass balance calculation can be performed to un-mix the $\delta^{33}S$ of labeled sulfide produced during the incubation period (Eq. 5, Fig 1.3).

$$\text{Total } \delta^{33}S = \text{Amount of } H_2S_{label} * \delta^{33}S\text{-}H_2S_{label} + \text{Amount of } H_2S_{old} * \delta^{33}S\text{-}H_2S_{old} \quad \text{Eq. 5}$$

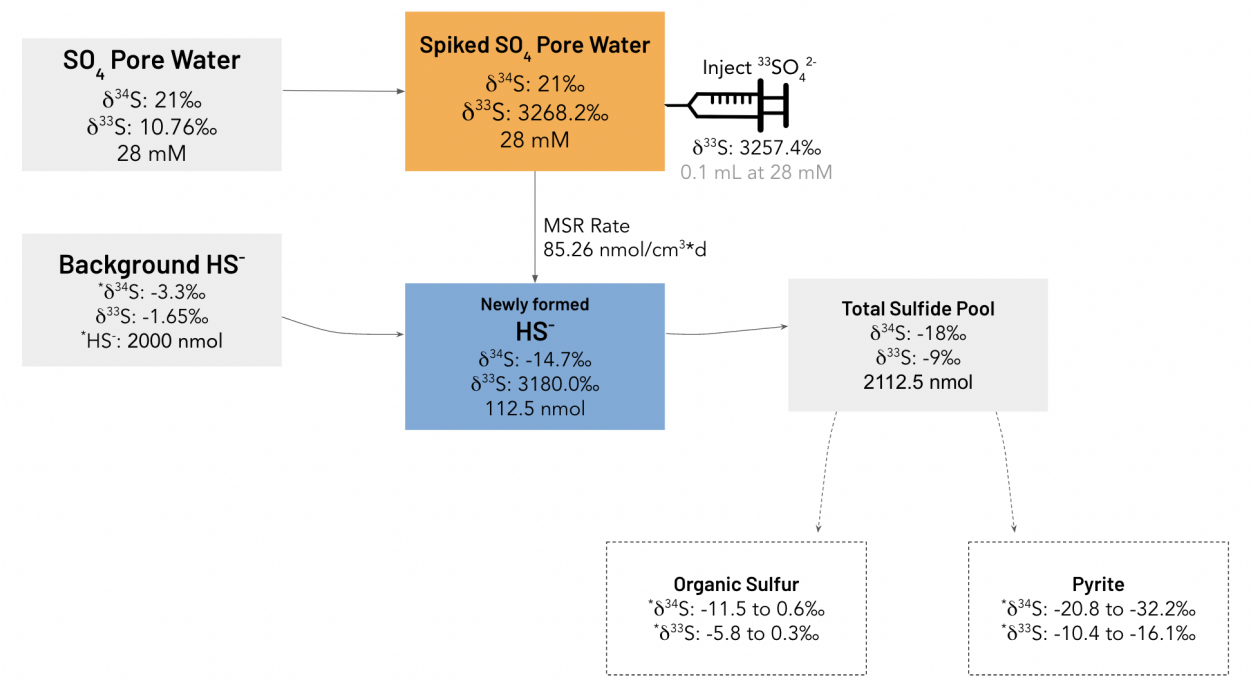

Figure 1.3 Flowchart of mixing and unmixing $\delta^{33}S$ and $\delta^{34}S$ values. The 33-S label is mixed into a background marine pore water/sediment sample, and then recovered in a total sulfide pool. Fractionations which occurred during the incubation period are shown in the blue box. Asterisks indicate values cited from Raven *et al.* 2016.

To calculate the concentrations of select sulfur isotopes in a mixture there are three required inputs: $\delta^{34}S$, the volume, total concentration of sulfur in the seawater or pore water in a sample and the volume of the tracer label spike (Eq. 5). The amount of the initial ^{33}S-SO_4 tracer is calculated from Equations 5-7.

$$^{33}S_{label}\ (\mu mol) = 0.98 * Vol_{label} * [SO_4]_{label} \qquad \text{Eq. 6}$$

To calculate the separate or "unmixed" absolute amount in moles of each isotope within the sample use Eq. 6, which uses the previously calculated $\delta^{33}S$, $\delta^{34}S$, and $\delta^{36}S$ values. Equations 6 and 7 assume that ^{36}S behaves mass dependently in proportion with $\delta^{34}S$.

$$^{3x}S_{sample}\ (\mu mol) = {}^{total}S_{sample}\ (\mu mol) * (^{3x}S/^{32}S)_{sample} * (^{32}S/^{tot}S)_{sample} \qquad \text{Eq. 7}$$

where

$$(^{32}S/^{tot}S)_{sample} = {}^{32}S_{sample} / [{}^{32}S_{sample} + {}^{33}S_{sample} + {}^{34}S_{sample} + {}^{36}S_{sample}]... \quad \text{Eq. 8}$$
$$= 1 / (1 + (^{33}S/^{32}S)_{sample} + (^{34}S/^{32}S)_{sample} + (^{36}S/^{32}S)_{sample})$$

Calculating the rate of sulfide production utilizes a sample's $\delta^{33}S$ value and the concentration of dissolved sulfate and sulfide (AVS). AVS contains both background initial sulfate and sulfides formed during the incubation with an added ^{33}S-labeled sulfate tracer.

Epsilon is the difference between the S-isotope compositions for MSR products and reactants. Alpha, $^{34}\alpha$ and $^{33}\alpha$, are kinetic fractionation factors defined by the ratio of rate constants specific to the isotopes (Hayes 2004). In the case of sulfur isotopes, enzymatic processes during MSR will produce fractionation factors which can be calculated using Eq. 9a and 9b.

$$^{34}\alpha = 1 + \varepsilon_{MSR}/1000 \quad \text{Eq. 9a}$$
$$^{33}\alpha = (^{34}\alpha - 1)^{0.515} + 1 \quad \text{Eq. 9b}$$

Equations 9a and 9b assume that even in diverse environments the $\Delta^{33}S$ values of the MSR-derived sulfide pool are not sensitive to ε_{msr}. To calculate the fractionation which occurred during the incubation period use Eq 10.

$$\Delta^{33}S = \delta^{33}S_{H2S\ Final} - \delta^{33}S_{H2S\ Intial} \quad \text{Eq. 10}$$

Example calculations using numerical values in the Supplemental section as Table 1.4.

Table 1.4 Step by step example of rate and epsilon recovery.

Step	Description	Input	Eq.	Output
1	Measure sulfur isotope abundances in AVS	Amount of ^{32}S ^{33}S, ^{34}S	Eq. 2a Eq. 2b	$\delta^{34}S_{Mix}$, $\delta^{33}S_{Mix}$

	fraction, calculate $\delta^{34}S_{sulfide,}$ $\delta^{33}S_{sulfide}$			
2.	Calculate Rate	nmol $^{33}S_{Label}$, volume of sediment, time of incubation	Rate = nmol $^{33}S_{Label}$ / sediment segment (cm^3)· incubation time (d)	nmol · cm^{-3}· d^{1-}
3.	Subtract out $\delta^{34}S_{sulfide}$ values for accumulated $\delta^{34}S\text{-}H_2S$	$\delta^{34}S_{Mix}$, $\delta^{34}S\text{-}H_2S$	$\delta^{34}S_{Label} = \delta^{34}S_{Mix} - \delta^{34}S_{sulfide}$	$\delta^{34}S_{Label}$
4.	Convert $\delta^{34}S\text{-}H_2S$ from previous published values into $\delta^{33}S\text{-}H_2S$. Subtract out $\delta^{33}S\text{-}H_2S$ values to calculate unmixed value of $\delta^{33}S\text{-}H_2S$	$\delta^{33}S_{Mix}$, $\delta^{34}S\text{-}H_2S$	$\delta^{33}S \approx \delta^{34}S/2$ $\delta^{33}S_{Label} = \delta^{33}S_{Mix} - \delta^{33}S_{sulfide}$	$\delta^{33}S_{Label}$
5.	Calculate epsilon	$\delta^{34}S_{Label,}$ $\delta^{33}S_{Label}$	Eq. 4	ε_{MSR}

1.2 Radiotracer $^{35}SO_4^{2-}$

Measuring SRR with a tracer is based on a simple concept —offering labeled sulfate to a population of sulfate-reducing bacteria and quantifying the amount labeled sulfides produced over a specified period of time. For close to eight decades, radiotracer, $^{35}S\text{-}SO_4^{2-}$, has been used to measure the rates of MSR in sediment cores from the seafloor. Sulfur-35 is a beta emitter with a half-life of 87 days and decays into ^{35}Cl (Jorgensen 2021). The origins of radiotracer $^{35}SO_4^{2-}$ were first described by Voge (1939) in a study deriving the rate of sulfate reduction over a set incubation period by using injecting ^{35}S labeled sulfate into pore water then measuring sulfate turnover rate. For each measurement, only a few hundred kBq ^{35}S sulfate is typically required, which has the detection limit of about 1 %, or equivalently a one hundredth of the total pore water sulfate

concentration if measured by ion chromatography (Jorgensen 2021). The first *in situ* use of ^{35}S-SO_4^{2-} was first demonstrated by Jørgensen *et al.* (1979) as 'whole-core incubation', where radiolabel was injected directly into sediment cores. This method has since been advanced by Westrich (1983), Kallmeyer *et al.* (2004) and Røy *et al.* (2014). A detailed timeline of the radiotracer's development history is listed in Section 1.4.

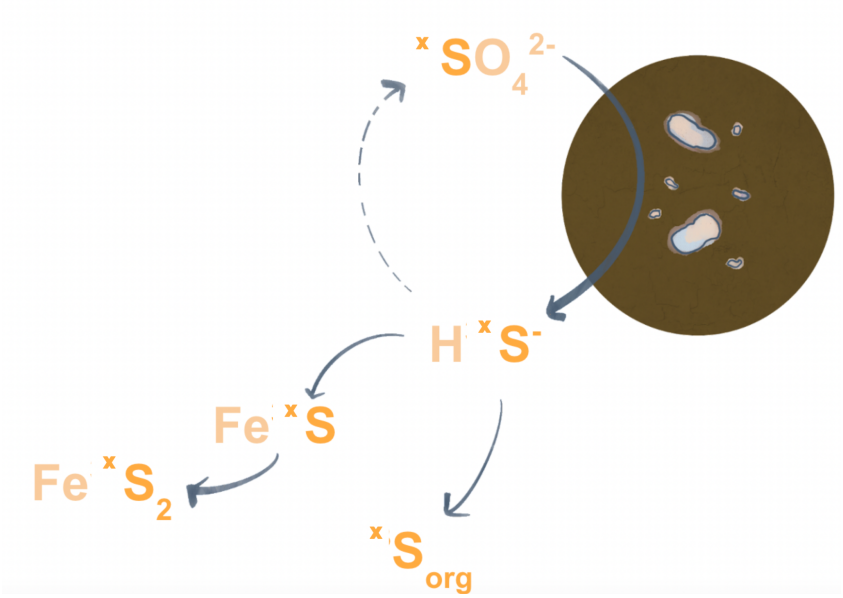

Figure 1.4 Visualization of sulfur cycle with labeled sulfate. ^xS represents ^{35}S or ^{33}S. The brown circle represents SRB.

In a real environment where factors such as species diversity, bacterial population density, availability and type of carbon substrate, and growth conditions are in flux, a tool to measure ε_{MSR} produced during a controlled *in situ* incubation experiment provides an entirely novel perspective on the range of fractionation values associated with a short (<24 hour) time frame which can then be compare to with $^{34}\delta S$ (‰) values associated with sulfur in later stages of the sedimentary sulfur cycle.

1.3 Brief Timeline of Radiotracer $^{35}SO_4^{2-}$

1939 Radioactive 35-S as described by Voge (1939) to trace the bulk composition of fractionation occurrences in a sample.

1979 'Whole-core Incubation' which was first demonstrated by Jørgensen *et al.* (1979), ^{35}S Radiotracer experiments showed a sulfur cycle that was very open to diffusional exchange as opposed to the original thought that a closed system between subsurface sediment and seawater. Additionally, Haworth (1979) ^{35}S-Sulfide with addition of HCl is in AVS, but does not extract oxidized forms pyrite and elemental sulfur. Particularly an issue when it comes to marsh sediments where pyrite was found to hold more of radiolabel than AVS fraction.

1973 Trudinger and Chambers (1973) first use of ^{35}S using sulfate reducing pure culture.

1983 Westrich (1983), first 35-S study done sequentially extracting labeled AVS and CRS.

1984 Howarth and Jørgensen, (1984): Reduced ^{35}S fraction underestimated by ~19%, Early studies are underestimating rapid pyrite formation during incubation.

1985 King *et al.* (1985): 50% of reduced 35S was in CRS fraction in salt marsh sediments, Early studies are underestimating rapid pyrite formation during incubation.

1986 Canfield *et al.*, (1986): Aqua regia extraction is found to contaminate reduced 35-S extracts leading to overestimations of reduced 35-S and thus removed from the method.

1989 Thode-Andersen and Jorgensen, (1989): CRS fraction is between 15-70%, low amounts of CRS are associated with high SRR and high sulfide concentration. Conclusion: Physical isotope exchange between reduced sulfur influences 35S distribution independent from rate of formation.

1998 Greeff *et al.,* (1998): Developed a free-falling benthic lander equipped to perform

pre-programmed sediment coring, 35S sulfate injection, in situ incubation, core retrieval, and finally ascent and onboard collection of incubated cores. Rates of in situ vs. on board experiments were relatively the same, meaning that hydrostatic pressure up to 200 bar did not have an effect on the metabolic rate, but oxygen uptake of marine sediments in the on board core exceeded in situ core.

2004 Kallmeyer *et al.*, (2004) increased efficiency of whole core incubation set up, introducing shorter incubation times, and the use of less radiotracer.

2014 Røy *et al*., 2014 : Microbes respond immediately and irreversibly to changes in their environment: by transitional warming of cold sediment, incidental introduction of oxygen, loss of sulfide, or contamination by surface sediment when coring deeper subsurface sediments.

Chapter 2. Pure Culture Incubations

2.0 Chapter Introduction

Pure culture incubations are a powerful tool in understanding fractionations as a function of cell specific rates of sulfur reduction (csrrR) without the additional abiotic complexities that come with real-life environments. For this reason, the first step in establishing the framework for $^{33}SO_4^{-2}$ is to vary as little biotic and abiotic conditions as possible to isolate whether or not the uptake of $^{33}SO_4^{-2}$ during MSR is the same as $^{35}SO_4^{2-}$. In this experiment, pure culture *Desulfovibrio vulgaris Hildenborough* (DvH) was grown in lactate (22mM)/sulfate (21.1mM) and incubated with $35\text{-}SO_4^{2-}$ (1 uCi/60mL) or $33\text{-}SO_4^{2-}$ (28 mM). Sulfur reduction rates (SRR) recovered by the radiolabel are directly compared to the SRR captured by $^{33}SO_4^{2-}$ and abiotic controls.

2.1 Pure Culture Incubation Methods

Media

Desulfovibrio vulgaris Hildenborough (DvH) was grown at 30°C in lactate (22mM)/sulfate (21.1mM) media (Table 2.1) under anaerobic conditions in 60 ml serum bottles. For experiment bottles, 1mL of resazurin in 2 liters of media was added as an indicator of O_2. No resazurin was added to media used for growth curve purposes to avoid complications in uneven coloring after the media was exposed to oxygen during transfer creating inconsistent absorbance measurements independent of the optical density of the culture (see Figure 2.3D). Media was acidified to a pH of ~7.3 using filter sterilized 6N HCl. Oxygen was removed from the headspace and media using 100% N_2 for 25 minutes plus the addition of Ti reductant.

Table 2.1. Detailed DvH Media Recipe

Chemical	Concentration	Chemical	Concentration
$NaHCO_3$	59.5 mM	$CaCl_2 \cdot 2H_2O$	0.6 mM
$Na_3SO_4 \cdot 10H_2O$	21.1 mM	Lactate	22 mM
KH_2PO_4	1.47 mM	*W-Se Solution	0.1 mM
NaCl	17.1 mM	*Trace Element Solution	1 mM
$MgCl_2 \cdot 6H_2O$	8 mM	*Vitamin Solution	20 mM
KCl	6.7 mM	NH_4Cl	20 mM

*W-Se Solution (Na2WO4·2H2O, Na2SeO3·5H2O, NaOH, ultrapure water), *Trace Element Solution (HCl, FeCl2·4H2O, CoCl2·6H2O, MnCl2·4H2O, ZnCl2, H3BO3, Na2MoO4· 2H2O, NiCl2· 6H2O, CuCl2 ·2H2O, ultrapure water), *Vitamin Solution (Biotin, Folic Acid, Pyridoxine-HCl, Thiamine-HCl, Riboflavin, Nicotinic Acid, D-Ca-pantothenate, Vitamin B12, p-Aminobenzoic acid, Lipoic acid, ultrapure water).

Growth Curve

Bottles were inoculated at 10% (vol/vol). Cell growth was measured using optical density (OD) at 600 nm over the course of 77 hours. For each OD measurement, one milliliter of inoculated media was removed using a syringe sparged using 100% N_2, transferred into a 1.5 mL cuvette, and measured using a Pharmacia Biotech Novaspec II. All absorbance measurements were "blanked" to uninoculated media at 600 nm.

Incubation Experiment

A series of 12 bottles were used (Table 2.2) : three replicates for each tracer, $^{33}SO_4^{2-}$ and $^{35}SO_4^{2-}$, three abiotic bottles, and three killed control bottles. All biotic bottles were inoculated and left to grow at 30°C without light. After four hours, replicate bottles and labeled killed controls and labeled abiotic bottles were injected with either 500 uL of $^{35}SO_4^{2-}$ at 1 µCi per bottle using a 1000 µL glass syringe or 100 µL of $^{33}SO_4^{2-}$ at 28 mM using a 100 µL glass syringe.

Initial sulfate concentrations were sampled anoxically from all bottles using a syringe pre gassed with 100% N_2 then transferred into 15mL conical vials using 2 µm filter which contained 0.5mL of 4N HCl to volatilize any H_2S. With the addition of labels marked the start of the incubation period which was recorded to the minute for each bottle.

Table 2.2 Bottle key for pure culture incubations with radiolabeled and stable isotope labels.

Bottle Name	# Replicates	DvH Culture	Label
Kill Control + Label	2	Y	35, 33
Kill Control	1	Y	None
33-SO_4^{2-}	3	Y	33
35-SO_4^{2-}	3	Y	35
Abiotic	1	N	None
Abiotic + Label	2	N	35, 33

All “killed control” bottles received 40mL of 20% zinc acetate to kill the microbial population within three minutes after the incubation period began. Incubation with the label occurred for 4 hours without light at 30°C, bottles were occasionally agitated with gentle shaking. At 8 hours from inoculation, final sulfate concentrations were sampled using the same procedure, then 40 mL of 20% N_2-sparged zinc acetate was added to bottles containing live cultures and abiotic controls to cut off microbial activity. This allowed sulfides produced during the incubation period to react with zinc acetate to form a solid white precipitate, ZnS. After 1 hour, bottles were opened, and contents were centrifuged in separate conical vials. Excess media was poured off the solids and remaining sulfides were transferred into round bottom flasks for AVS. For a detailed procedure of AVS see Section 2.1. Total sulfate concentrations for nonradioactive samples were quantified using $BaCl_2$ precipitated to $BaSO_4$. The amount of sulfate was calculated using the mole ratio of SO_4:$BaSO_4$ from the mass of the precipitate.

Following AVS extraction, sulfides were oxidized to sulfate using 30% hydrogen peroxide (Hoffmann 1977, see section 3.1 for more detail) then quantified using Metrohm 930 Compact IC using a Metrosep A Supp 100/4.0 column and isocratic eluent (0.32 M Na_2CO_3: 0.1 M $NaHCO_3$) at a flow rate of 0.7 mL/min.

Concentrations of radioactively labeled sulfides were determined using a scintillation counter. The scintillation counting efficiency of 35-S is 97%, so 1 μCi corresponds to 2.22×10^6 cpm. The activity of the original material was 1.72 mCi (115 cpm/μl). Samples were run in a window from 0.1-167 keV, for 5 minutes using a Beckman LS 6500 Scintillation Counter. Initial sulfate, final sulfate and AVS sulfide samples were diluted to 5 mL (for example, 0.5 mL of sulfate was diluted with 4.5 mL of ultra pure water) and 14.5 mL of scintillation fluid. A full procedural flowchart from inoculation to final data collection is visually laid out in Figure 2.1.

Figure 2.1. Flowchart of method for pure culture incubations. followed for processing bottles containing 33-sulfur and 35-sulfur labels for pure culture incubation experiments.

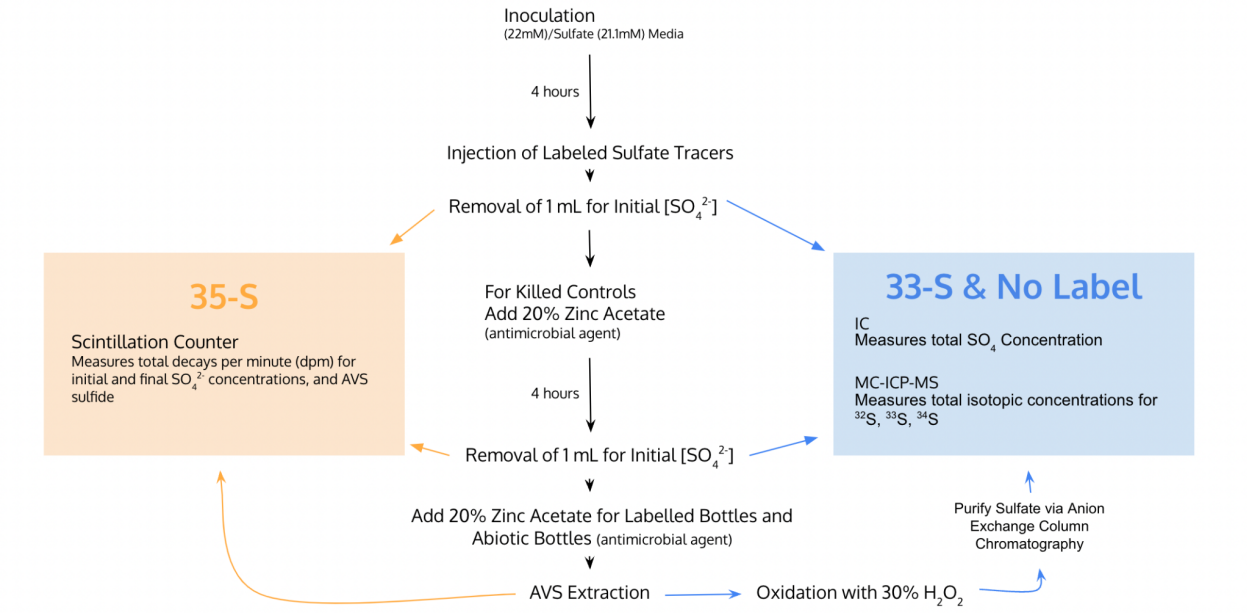

2.2 Results and Discussion

Growth Curve

Growth rates were estimated by plotting logarithmic optical density at 600 nm over time from 3 replicate bottles. Time points were taken with a minimum of 4 hours in between to allow time for any potential oxygen introduced during the sampling process to reoxidize H_2S to SO_4^{2-}. DvH has a moderate aerotolerance which allows for high survival rates should accidental oxidation occur (Wildschut et al. 2006, Ramel et al. 2015, Ramel et al. 2013, Yurkiw et al. 2012). However, time points taken hourly within the first 16 hours of growth introduced too much oxygen causing the anaerobes to die (Figure 2.3E). If this curve is to be repeated in higher resolution, the inoculated media should be interacted with as little as possible by either observing growth in a hungate tube with optical glass or extracting individual aliquots in an O_2-free glove bag during the first 16 hours of growth. A detailed account of all growth curve trials and their individual issues is listed in

Figures 2.3A-E. The exponential growth for DvH occurred within the first 20 hours of inoculation with a growth rate of 0.12 hr^{-1} and a doubling time of 5.6 min. These observations fall in line with OD_{600} growth curves produced by Ramel *et al.* (2015), Johnson *et al.* (1997), Mukhopadhyay (2006), Borglin *et al.* (2008) (Table 2.3). The growth rate (μ) was calculated using Eq. 11 where OD is indicative of the $\log(OD)_{600}$ at the start (OD_1) and end (OD_2) in the linear portion on the y-axis divided by the corresponding age (T_1, T_2) on the x-axis. The doubling time was calculated using Eq. 12.

$$\text{Growth Rate, } \mu = (\ln [OD_2/OD_1]) / (T_2-T_1) \qquad \text{Eq. 11}$$

$$\text{Doubling Time} = \ln(2)/\mu \qquad \text{Eq. 12}$$

Table 2.3 Comparison of growth rate and doubling times measured by this experiment and literature values: Ramel *et al.* (2015), Johnson *et al.* (1997), Mukhopadhyay (2006), Borglin *et al.* (2008) with DvH grown in medium C and optical density measured via hungate tubes.

	Growth Rate, μ (hr^{-1})	Doubling Time (hr)
Ramel *et al.* (2015)	0.13	5.21
This Study	**0.12**	**5.62**
Johnson *et al.* (1997)	0.12	5.77
Mukhopadhyay (2006)	0.09	7.52
Borglin *et al.* (2008)	0.08	9.00

While the growth rate and doubling times of this experiment's cultures reflect literature values, the culture did not grow to the anticipated maximum optical density. The semilog of optical density at 600 nm reached a maximum of 0.12 which is a fraction of the optical density is typically a max $\log(OD)_{600}$ at 0.89-1.00 (Ramel *et al.* 2015, Johnson *et al.* 1997, Mukhopadhyay 2006,

Borglin *et al.* 2008). This may point to issues with the media content where a nutrient, such as phosphorus, could be exhausted as the culture reached an OD of 0.1 limiting future growth.

In future experiments, it's recommended all salts should be filtered and sterilized instead of being autoclaved to reduce the possibility of heat inactivation. Additionally, no precipitate should be visible in the media prior to inoculation. The media used in this experiment did have some visible solids which were salts that fell out of the solution over time. Decreasing the concentration of salts should improve solubility. Ramel *et al.* (2015) uses a lower media concentration at liquid lactate (37mM)/ sulfate (32mM) medium which may be of relevance to future alterations of this procedure.

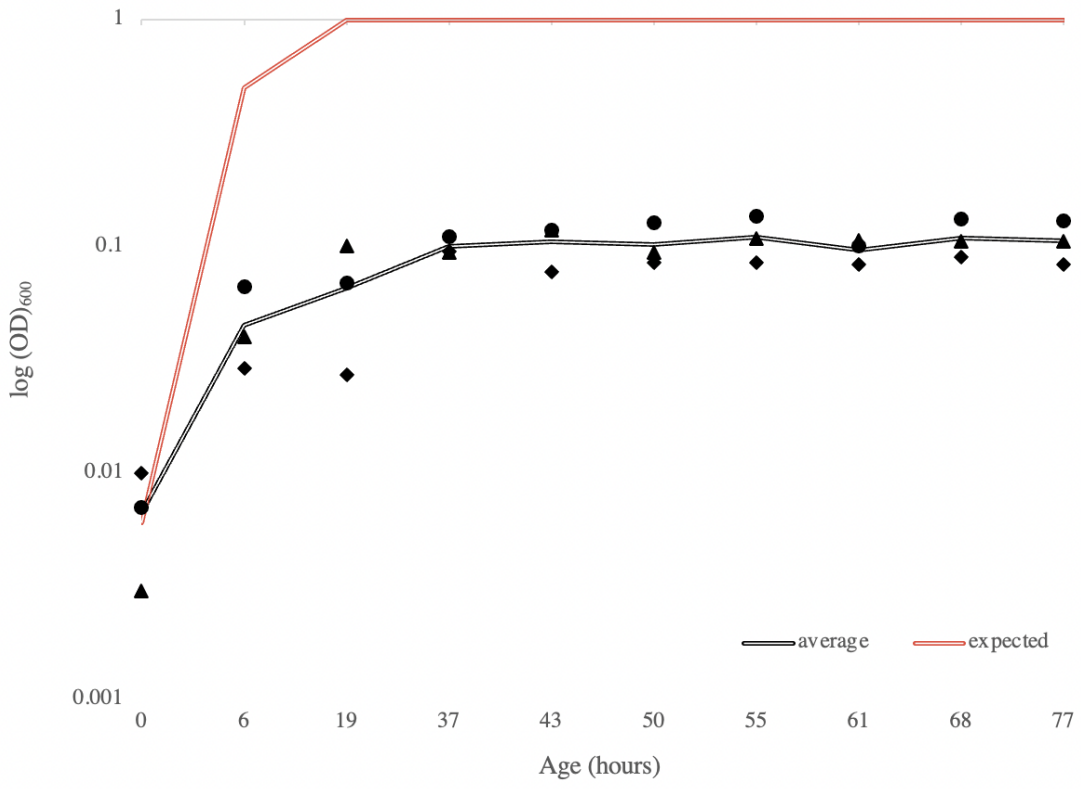

Figure 2.2. Semilog plot of the growth of *Desulfovibrio vulgaris* Hildenborough (DvH). Optical density was measured at 600 nm. DvH was grown anaerobically at 30°C in 60 mL serum bottles in lactate (22mM)/ sulfate (21.1mM) medium (see Table I for details) and sampled in 1.5 mL cuvettes. The expected curve is roughly estimated using the starting average OD of the media and the maximum optical density maximum measured by Ramel *et al*. (2015) and Johnson *et al.* (1997).

Figures 2.3A-E Growth curve DvH trials and their issues.

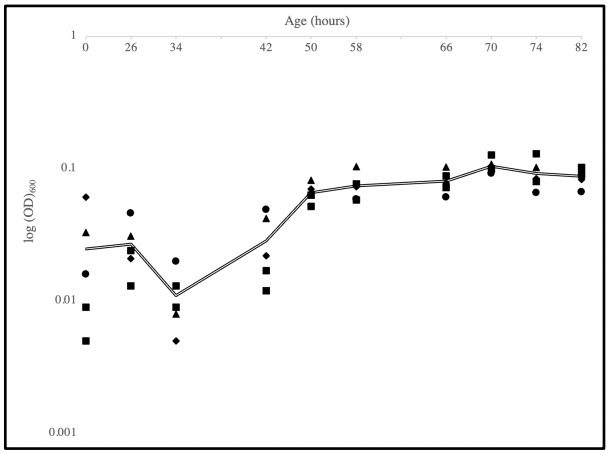

Fig 2.3A.
Used 10 mL hungate tubes, Inoculated at 10% v/v.
Issues: Non-optical glass lead to noisy data. Six replicates. Noise from 0-42 hours may also be a result of very low optical density which should have looked minimal in comparison to the final density which was expected to be 1.0.

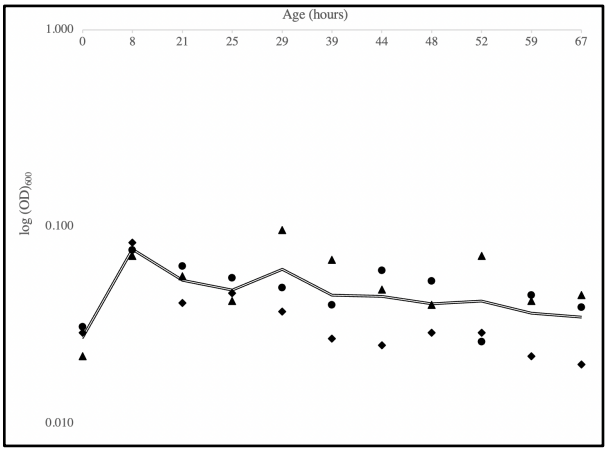

Fig 2.3B.
Used 10 mL hungate tubes, Inoculated at 10% v/v.
Issues: Did not shake/agitate the tubes enough leading to under-measuring the absorbance. Plus noise from non-optical glass.

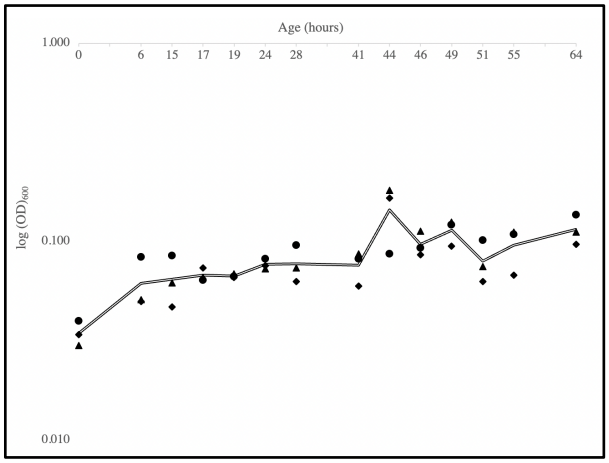

Fig 2.3C.

Used 10 mL hungate tubes, Inoculated at 10% v/v.
Issue: Non-optical glass lead to noisy data (basically a retry of curve 1 without actually fixing anything).

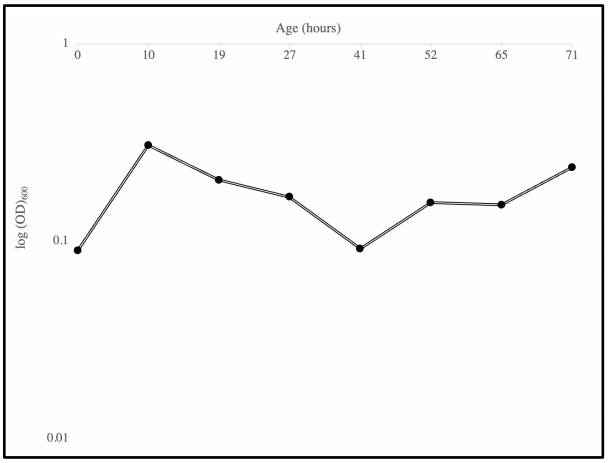

Fig 2.3D.
Used 60mL serum bottles. Inoculated at 10% v/v. Only one replicate was used because I wasn't sure how the resazurin would work out.
Issue: Impossible to keep media culture aliquots the same color because the resazurin would only partially oxidize and never at a consistent rate so there would be an irregular array of pink/translucent shades. Could not compare absorbances to the blank. Resauzurin (in the presence of O_2) also changes color with age.

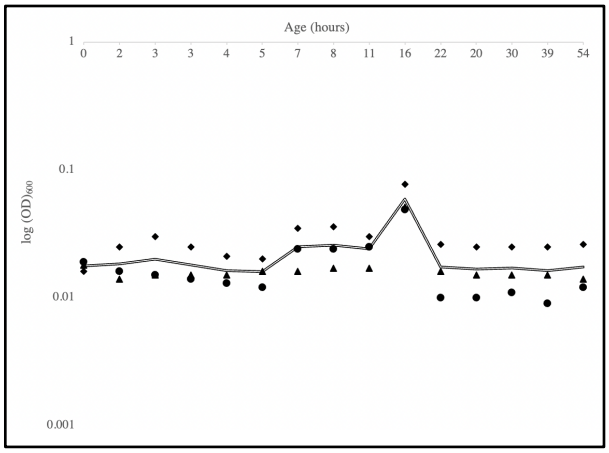

Fig 2.3E.
Used 60mL serum bottles. Inoculated at 10% v/v.
Issue: This curve I did because I wanted a higher resolution version of Curve 5. The set-up was the same as curve 5, but I think taking time points every hour introduced too much O_2 overtime from the motion of sticking the syringe needle into the stopper and potential O_2 in the syringe needle's headspace. This wasn't an issue in any of the previous curves because the time between each sampling point was enough to where the O_2 could reoxidize H_2S and/or was at a low enough concentration that the DvH could tolerate it. Culture died after 15.5 hours.

Sulfate Reduction Rates

The direct comparison of SRR measured using sulfide abundance in $^{33}SO_4^{2}$–labeled bottles (SRR-33) and $^{35}SO_4^{2-}$ (SRR-35) in units of nmol/mL*day is plotted in Figure (2.4). The pink dot indicates killed controls which formed sulfide for hours 0-4 before receiving 40 mL of 20% zinc acetate. The amount of sulfide produced within the killed control bottles is based on SRR during the first four hours from inoculation. The replicate label bottles show SRR with the label from hours 4-8 from inoculation, any sulfide produced during 0-4 hours is unlabelled.

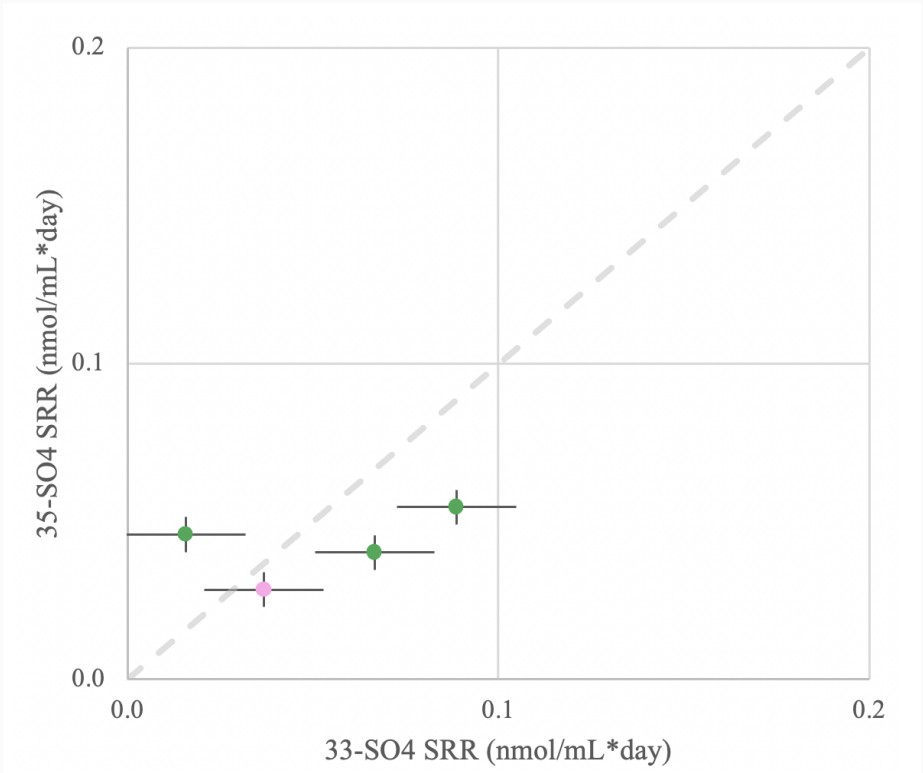

Figure 2.4 Comparison of SRR 35 (nmol*mL^{-1}*day^{-1}) versus SRR 33 (nmol*mL^{-1}*day^{-1}) with *DvH* pure culture. Green dots are label replicates. Solid pink dot is labeled killed control. Outlined pink dot is kill control bottles with no label. Gray dotted line marks 1-1 ratio.

Sulfates measured in labeled abiotic control bottles were subtracted out of the total oxidized AVS sulfides for each of the respective labeled experiment bottles in order to estimate the sulfide that was produced solely from MSR. The total amount of sulfide measured in the abiotic bottles was 0.010 µmol for abiotic-33, 2.296 µmol for abiotic-35, and 0.0005 µmol for abiotic-no label (Table 2.4). The presence of sulfides in the AVS fractions is likely an accumulation of a procedural SO_4^{2-} blank from the AVS line and the addition of H_2O_2 which was averaged to be 2.00±0.454 nmols for three blanks (Table 5.1) which makes up 20% of the sulfide recovery from the average 33-S labeled bottle. Abiotic-35 bottles have a known sulfate blank of 2.294 µmol in 60 mL of media which is hypothesized to come from the cross-contamination of 35-SO_4^{2-}. Future repetitions of this experiment should include a swipe test for radiation contamination, and an additional sulfate blank run during scintillation counting made up of MilliQ water and scintillation fluid to confirm that additional sulfate is not present in the scintillation fluid.

Table. 2.4 Pure culture incubations results. For the first trial of the experiment, 30 mL of 20% zinc acetate was used to kill microbial population for biotic bottles and kill control. The second trial used 40 mL of 20% zinc acetate. X,Y, and Z refer to replicate 35-S bottles. A, B, and C refer to replicate bottles with 33-S. Sulfides for 33-S and abiotic bottles were not recovered for Trial 2.

	Trial	Initial SO_4^{2-} (uCi/mL)	Final SO_4^{2-} (uCi/mL)	Total H_2S (uCi)	Sulfate Turnover (%)	Percent Recovery (%)	**Labeled** SRR (nmol*mL^{-1}*day^{-1})
Killed Control 35	1	1.24	0.916	0.00170	26%	86%	0.1144
	2	1.16	1.13	0.00384	2%	98%	0.2580
35-SO_4^{2-} (X)	1	2.50	1.89	0.00151	24%	81%	0.1017
	2	1.22	1.03	0.00401	15%	85%	0.2698
35-SO_4^{2-} (Y)	1	1.40	1.29	0.00173	7%	103%	0.1163
	2	1.21	1.15	0.00423	4%	96%	0.2843
35-SO_4^{2-} (Z)	1	1.36	1.16	0.00268	14%	102%	0.1803
	2	1.32	1.28	0.00410	3%	97%	0.2755
Abiotic 35	2	0.91	0.88	0.00342	3%	97%	0.2296
	Trial	Initial SO_4^{2-} uM	Final SO_4^{2-} uM	Total H_2S umol	Sulfate Turnover (%)	Percent Recovery (%)	**Total** SRR (nmol*mL^{-1}*day^{-1})
Killed Control	1	2480	2300	0.0398	7%	93%	2.2580
	2	2745	2510		9%		
Killed Control 33	1	2661	2621	0.226	2%	98%	2.9781
	2	2354	2378		0%		
33-SO_4^{2-} (A)	1	2285	1987	0.041	13%	87%	4.0564
	2	2521	2009		20%		
33-SO_4^{2-} (B)	1	2321	1715	0.0537	26%	74%	5.3732
	2	2680	1948		27%		
	1	2580	1960	0.0099	24%	76%	0.9926

33-SO_4^{2-} (C)	2	2709	2040		25%		
Abiotic	1	2134	2178	0.0010	0%	102%	0.1009
	2	2153	2345		0%		
Abiotic 33	1	2711	2603	0.0005	4%	96%	0.0537
	2	2403	2060		14%		

Sulfate Turnover (%) = ($^{3x}SO_4^{2-}{}_{INTIAL}$ - $^{3x}SO_4^{2-}{}_{FINAL}$) / $^{3x}SO_4^{2-}{}_{INTIAL}$ * 100 Eq. 13

Percent Recovery (%) = ($^{3x}SO_4^{2-}{}_{FINAL}$ + $^{3x}H_2S_{TOTAL}$) / $^{3x}SO_4^{2-}{}_{INTIAL}$ * 100 Eq. 14

SRR = (amount of H_2S)/ (volume * time of incubation) Eq.15

The main objective of this experiment was to compare sulfate reduction rates of $^{33}SO_4^{2-}$ to those of $^{35}SO_4^{2-}$ by pure culture *Desulfovibrio vulgaris Hildenborough* (DvH) in parallel bottle incubations. SRR-33 rates were calculated using Eq. 15 where the amount of H_2S was the total AVS recovered (umols) in a volume of 60 mL of media over 4 hours. SRR-35 is the amount of 35-S radioactivity converted to umol using a conversion factor of 1488 Cu/mmol of sulfur in a volume of 60 mL of media over 4 hours. Procedural AVS and H_2O_2 blanks for 33-S, and 35-S bottles were removed using the AVS recovered in 35-Abiotic and 33-Abiotic bottles. The ratio of rates between total AVS in SRR-33 and SRR-35 is scattered on either side of the 1-1 line with error bars based on uncertainty in MSR rate (nmol*mL^{-1}*day^{-1}) which do not cross the 1-1 line, the averaged srr-33:SRR-35 ratio of 0.98±0.34 for three replicates of 35-S and 33-S bottles. The uncertainty was calculated using the standard deviation of 33-S and 35-S replicate bottle values. These results are inconclusive as to whether there is difference in uptake by either label during

MSR, but we find no evidence for a systematic or directional bias between the two techniques. To improve precision on SRR values for both tracers additional repetitions of the experiment and swipe-tests for 35-S cross contamination. In conclusion, the preliminary rate comparisons of this experiment suggest the potential interchangeable nature of $^{35}SO_4^{2-}$ and $^{33}SO_4^{2-}$ for SRR measurements, but more repetitions of this experiment are required.

Cell Specific Sulfur Reduction Rates

Cell-specific sulfur reduction rates (csrrR) are required in the next trials of this experiment in order to make direct comparisons of rate with $^{33}SO_4^{2-}$ with unlabeled SO_4^{2-} with other DvH experiments and pure cultures from various environments (Table 2.5). Actual measurements of sulfur isotope distributions before and after the incubation should be measured using ICP-MS, then epsilon values produced by DvH can be calculated and compared to literature values. The epsilon $^{34}\varepsilon$ (‰) previously published for lab cultured DvH are 15.9±0.4‰ (1σ) (Bertran *et al.* 2018), and 17.3 ± 1.5‰ (2σ) for wild-type strains from deep marine sediments (Leavitt *et al.* 2015) (Table 2.5).

Table. 2.5 Cell-specific sulfate reduction rates and fractionation factors of investigated sulfate-reducing prokaryotes. All species used lactate as electron donor. Natural environment data comes from Detmers *et al.,* (2001) and Sim *et al.* 2011, Bertran *et al.* 2018, Leavitt *et al. (2015).*

			$^{34}\varepsilon$ (‰)	csSRR (fmol cell^{-} day^{-})
Deep Ocean	submarine hot spring	*Archaeoglobus fulgidus strain Z*	17	63.8
	hydrothermal vent	*Desulfovibrio sp. strain X*	5.4	36
	deep sea sediment	*Desulfovibrio profundus*	4.1	17
	deep sea sediment	***Desulfovibrio vulgaris hildenborough***	17.3 ± 1.5	-
Terrestrial	aquifer	*Desulfotomaculum geothermicum*	8.1	12.5
	thermal vent water	Thermodesulfovibrio yellowstonii	17	24

	oil reservoir	*Desulfotomaculum thermocisternum*	15	310
	freshwater mud	*Desulfobulbus sapovorans*	16.5	26
	manganese ore	*Desulfomicrobium baculatum*	4.8	12.7
Coastal, Estuarial, Continental Shelf	saline sediment	*Desulfohalobium redbaense*	10.6	434
	arctic sediment	*Desulfotalea arctica*	6.1	4.2
	hypersaline matt	*Desulfovibrio oxyclinae*	4.5	69.1
	arctic sediment	*Desulfotalea psychrophila*	4.3	6.3
	hypersaline microbial mat	*Desulfovibrio halophilus*	2	33.1
Pure Culture		***Desulfovibrio vulgaris hildenborough***	15.9±0.4	75

To estimate csSRR rates, another growth curve is required measuring cell counts at each time point, or alternatively measuring the total cell count at the time of inoculation (0 hours), then at the time of label addition (4 hours), then after the incubation period (8 hours). Cell-specific sulfate reduction rates (csSRR, in moles $cell^{-1}day^{-1}$) can be calculated for the exponential phase using the change in concentration of sulfate and cell number (cn) between time points (T_1) and (T_2)(Eq. 16).

$$\mathrm{csSRR} = \frac{\mathrm{SO}^{2-}_{4(2)} - \mathrm{SO}^{2-}_{4(1)}}{\frac{(\mathrm{cn}_{(1)} + \mathrm{cn}_{(2)})}{2} \cdot (T_{(2)} - T_{(1)})} \qquad \text{Eq. 16}$$

2.3 Chapter Conclusion

In order to suggest $^{33}SO_4^{2-}$ as an alternative for $^{35}SO_4^{2-}$ sulfur reduction rates of both tracers were directly compared through parallel bottle incubations with well-studied pure culture *Desulfovibrio vulgaris Hildenborough* (DvH). The exponential growth for DvH occurred within

the first 20 hours of inoculation with a growth rate of 0.12 hr^{-1} and a doubling time of 5.6 min which reflect literature values (Ramel *et al.* (2015), Johnson *et al.* (1997), Mukhopadhyay (2006), Borglin *et al.* (2008). However, there may be an issue with the media as the maximum OD reached was 0.12 whereas literature values observed a max OD of 0.89-1.00 (Ramel *et al.* 2015, Johnson *et al.* 1997, Mukhopadhyay 2006, Borglin *et al.* 2008). The ratio of calculated sulfate reduction rates between the averages of all SRR-33: SRR-35 replicate bottles is 0.98±0.34. Because these values are scattered on either side of the 1-1 line demonstrating no clear bias for either label but these results are inconclusive as to whether there is difference in uptake by either label during MSR. To improve precision on SRR values for both tracers additional repetitions of the experiment and swipe-tests for 35-S cross contamination. The results of the pure culture incubations provide a preliminary argument for the interchangeable uptake of $^{35}SO_4^{2-}$ and $^{33}SO_4^{2-}$ by sulfate reducing organisms to measure SRR. This may become a valuable alternative in situations where the radiotracer cannot be used.

Chapter 3. Whole Core Incubations

3.0 Chapter Introduction

The second foundational step in establishing the $^{33}SO_4^{2-}$ method was to conduct parallel whole-core incubations in experiments in the environment. Santa Barbara Basin (SBB) was chosen for its sub-oxic setting which hosts an active SRB population (Reimers et al., 1996; Raven et al., 2016, Abdulla et al. 2020). SBB is located near-shore off the coast of Southern California and has been extensively studied for its varved anoxic marine sediments which provide an exceptionally well-defined paleo-oceanographic redox record. Sediment in the deep center of the basin (Fig 3.1) is almost completely laminated for preserving the past 2000 years (Schimmelmann *et al.* 2013). While high-resolution archival cores from SBB have been used for decades to reconstruct paleo-oceanographic redox conditions (Moffiet *et al.* 2014, Schimmelmann *et al.* 2013), modern sediments are heavily cited for their richness in OM (Abdulla *et al.,* 2020).

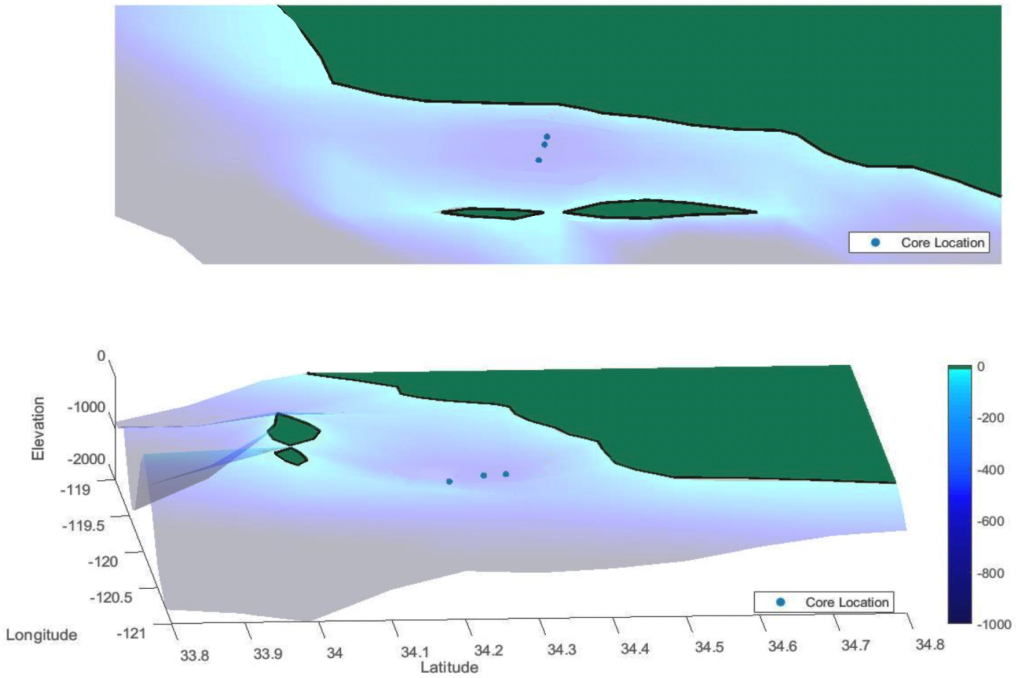

Figure. 3.1. Bathymetry of Santa Barbara Basin. Core locations (blue dots).

The basin is shallow with a maximum depth of 627 m and an average sill depth of 475 m (Bernhard & Reimers 1991). Average sedimentation rates at the deepest parts of the basin are 1.2-1.8 mm/yr (Behl, et al. 2007). Water circulation through the west side of the basin is heavily restricted due to the bowl-like bathymetry cushioned by the continental margin and Channel Islands. Seasonally, the basin is "flushed" with oxygenated water from the eastern side of the basin, the resultant mixing of water densities creates upwelling which causes productivity in the Santa Barbara Channel to bloom. Oxygen is quickly consumed when the downward flux of OM is consumed and remineralized through microbial respiration (Callbeck et al. 2021; Goricke 2015). This creates low concentrations of dissolved oxygen in the water column and dysaerobic bottom water. Outside of these seasonal "flushes", depths below the sill height of 470 m have bottom water dissolved oxygen concentrations <0.1 mL/L (Goricke 2015, Raven et al. 2016) (Figure 3.1). These conditions facilitate a host of sulfur reducing bacteria and archaea populations which steadily turn over dissolved organic and inorganic sulfur (Callbeck 2021).

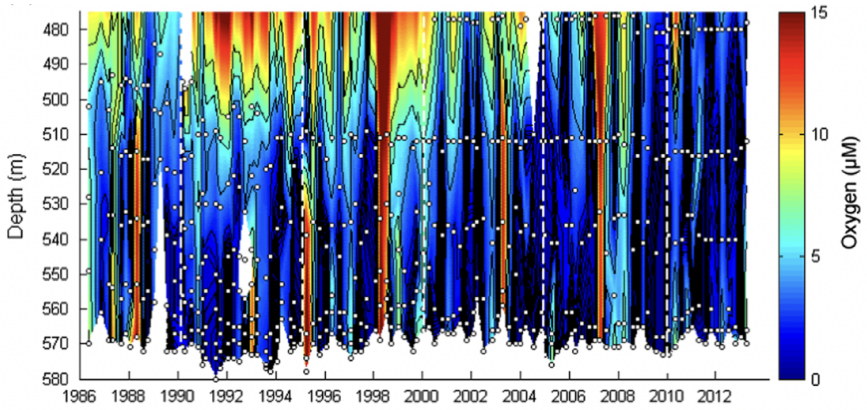

Figure. 3.2 Time-depth plots of dissolved oxygen and at the bottom of the SBB using data collected below 225 m. Dashed vertical lines are spaced at 5-year intervals to alignment of events. Goricke 2015, Elsevier.

3.1 Whole Core Incubation Methods

Core Collection

Parallel "twin" push cores were sampled at three different heights, 498.08 m, 572.51 m, and 572.55 m, all below the sill height (Figure 3.2). Core liners took 16 cm of sediment. After retrieval, cores were sub-cored to 0.5 cm diameter using a 60 mL syringe that was screwed into a port at the top of the core opening. As the liner was pushed into the sediment at an equal pace, pressure was drawn in the syringe so that the surface of the sub core and level of the outer push core sediment surface remained even. The top of the core liner contained 2-3 cm of bottom water overlying the sediment surface.

Injection of Tracer

Each 1-cm-interval sample was injected with tracer. At 1 cm intervals the label was injected at a steady rate by inserting the syringe needle as straight as possible into the center of the core. For $^{33}SO_4^{2-}$, 50μL of at 28 mM. For $^{35}SO_4^{2-}$, 100 μL of $^{35}SO_4^{2-}$ at 1 μCi per interval of sediment. Both labels were pre-sparged with 100% Ar for 20 minutes prior to injection. Tape was used to cover inlets on the side of the core liner. Cores were stored at 43°F (6°C) for 8 hours. Following the incubation period, cores were sliced into 1 mL intervals and transferred into an O_2-free conical vial containing 10 mL of 20% zinc acetate in water (wt/vol) which was pre-sparged with Ar for 20 minutes. Samples were centrifuged for 10 minutes at 4200 rpm, then frozen at -80°F. Two 1 cm intervals below the last injection depth were also extruded to determine label smearing effects which are not included in this study. Cores containing radiolabel were measured using scintillation counting.

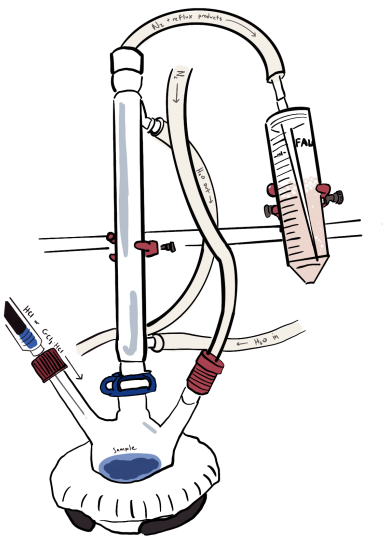

Extraction of Acid Volatile Sulfides (AVS)

Immediate products of MSR are defined as acid volatile sulfides (AVS) which encompass iron monosulfide, H_2S and HS^- /S^{2-} for pH conditions greater than 7. Sulfide (S^{2-}) and bisulfide (HS^-) have pKa_1 of 7.04 and pKa_2 11.96 respectively. This property makes porewater sulfides easily volatile under acidic conditions. The sediment and pore water mixture was acidified, releasing sulfides in the sample as H_2S gas which is then trapped in a secondary container as ZnS. The chemistry behind this process is listed below in Eq. 14.

$$HCl_{(aq)} + S^{2-}/HS^-_{(aq)} \rightleftharpoons H_2S_{(g)} + Zn^{II} + 2\ CH_3CO_2^- \rightarrow ZnS_{(s)} \qquad \text{Eq. 17}$$

To begin the extraction, the samples were thawed, weighed, and placed in a round bottom flask. One to two sulfide standards were also processed per four or five samples to check the quality of AVS extraction. Both the sample and the zinc acetate trap were purged with N_2 gas for 10 minutes. The sample was then acidified with 30 mL of 6N HCl and the mixture was heated and maintained at 60-70^{o}C. All H_2S gas was carried and trapped in a secondary falcon tube containing 25 mL of 5% zinc acetate. The physical set up of the reaction is pictured in Figure 4. In the trap, H_2S gas reacts with zinc acetate to form ZnS which is a white solid. The reaction proceeded to reflux for approximately 2 hours. After the reaction had finished, the falcon tube containing the newly formed ZnS was then capped and centrifuged. All zinc acetate was poured off into waste and the ZnS were washed thoroughly three times with ultra-pure water.

Figure 3.4. AVS and CRS reflux system and zinc acetate trap.
Typically, six identical set ups are linked to one line so that six

samples can be sequentially extracted at a time.

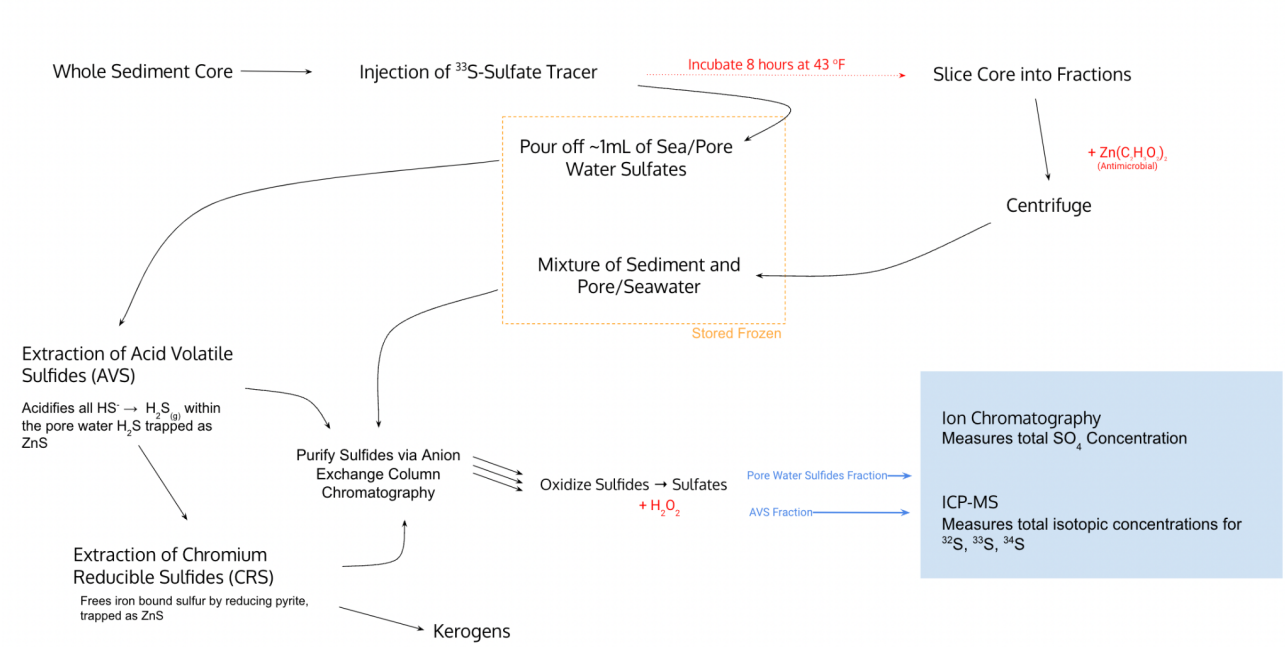

Figure 3.5. Flowchart of methods for whole core incubation with 33-SO_4^{2-}.

Oxidation of AVS

For all sulfide fractions including, porewater sulfides, and AVS extracted fractions must undergo oxidation into sulfates to be measured via ion chromatography and ICP-MS.

$$H_2O_{2\,(aq)} + ZnS_{(s)} \rightarrow ZnSO_{4\,(s)} \qquad \text{Eq. 18}$$

The oxidation process started with the addition of 3 mL of 30% H_2O_2 which was left to react at room temperature for ~1hr, then refluxed in its closed falcon tube at 60°C for >24hrs. The sulfate samples were then transferred to flat bottom 4 mL Teflon containers and dried down on a hot plate at 110°C for 12-24hours, a 2nd aliquot of H_2O_2 was added, then dried down for 12-24 hours until no liquid was visible.

Anion-Exchange Chromatography

All samples were processed through anion exchange column chromatography to remove any impurities with a charge (such as Cl^-) using BioRad AG-1-X8 strong anion resin which has a strong affinity to sulfate (Paris *et al.* 2013). This works by having two "working forms" : the nitric form and the chloride form. When the resin is flushed with SeaStar® HCl, the sulfates are trapped in the column while any other charged compounds are flushed out. The resin is conditioned thoroughly with alternating rinses with reagent grade (R.G.) 1.6 N HNO_3 , R.G. 3.3 N HCl, 0.5 N SeaStar® Baseline HNO_3, 3.3 N SeaStar® Baseline HCl and 0.165 N SeaStar® Baseline HCl. The sample was added to the column then flushed with 3.3 N SeaStar® Baseline HCl to wash out all charged compounds that were not sulfate. Then the purified sulfates flushed out of the column using ultrapure SeaStar® HNO_3 and collected in ultraclean Teflon containers and dried on a

hotplate at 100°C. The dried down purified sulfate aliquot can be diluted for spectrometry instruments.

Scintillation

Radiolabeled, ^{35}S, sulfide pore water aliquots from each depth interval were transferred into scintillation bottles. The bulk composition of the remaining ^{35}S was measured via scintillation in Ci/mL aboard AT42-19 by the Treude lab group from UCLA. Rates were described in terms of the unitless value k* (Eq. 7).

$$*k = DPM\ TRIS / (DPM\ TRIS + DPM\ Sulfate) / Time \qquad \text{Eq. 19}$$

3.2 Results and Discussion

Core Details

Table 3.1. Core site locations and depths.

DATE	EXPEDITION	SITE	$^{33}SO_4^{2-}$ Tracer Core	High Resolution Core	Archive Core	Latitude	Longitude	Water Depth (m)
5.NOV.19	AT42-19	NDT3-A	●	●	●	34.292171	-120.025552	572.51
6.NOV.19	AT42-19	NDT3-C	●	-	-	34.352602	-120.016151	498.08
9.NOV.19	AT42-19	SDT1-A	●	-	●	34.211952	-120.116487	572.55

Table 3.2. Core pictures and description from AT19-42 taken by Molly O'Beirne (Dec 2019).

SITE	Interval (cm)	Color	Sediment Type	Other	Core Picture
NDT3-C	0-2	Brown	Fluffy Surface		 NDT3-A
	2-3	Black	Liquid Mud		
	3-3.5	Gray Brown	Liquid Mud		
	3.5-8	Gray Black	Firm OM-rich		
	8-8.5	Black	Firm OM-rich		
	8.5-12	Gray	Firm OM-rich		
	12-16	Black	Firm OM-rich		
	Interval (cm)	Color	Sediment Type	Other	
NDT3-C	**0-2.5**	**Gray Brown**	**Liquid Mud**	**Amphipod in 0-1cm Interval**	 NDT3-C
	2.5-3	**Black**	**Clay**		
	3-11	**Gray Brown**	**Firm Clay**		
	11-11.5	**Black**	**Firm Clay**		
	11.5-17	**Gray Brown**	**Firm Clay**		

SDT1-A

Interval (cm)	Color	Sediment Type	Other
0-1	Green Brown	Liquid Mud - OM rich	
1-2	Gray Brown	Clay	
2-3	Green Brown	Firm OM-rich	
3-7	Gray Brown	Clay	
7-7.5	Black	Clay	
7.5-9.5	Gray Brown	Clay	
9.5-10	Black	Clay	
10-16	Gray Brown	Clay	

SDT1-A

Porewater Chemistry

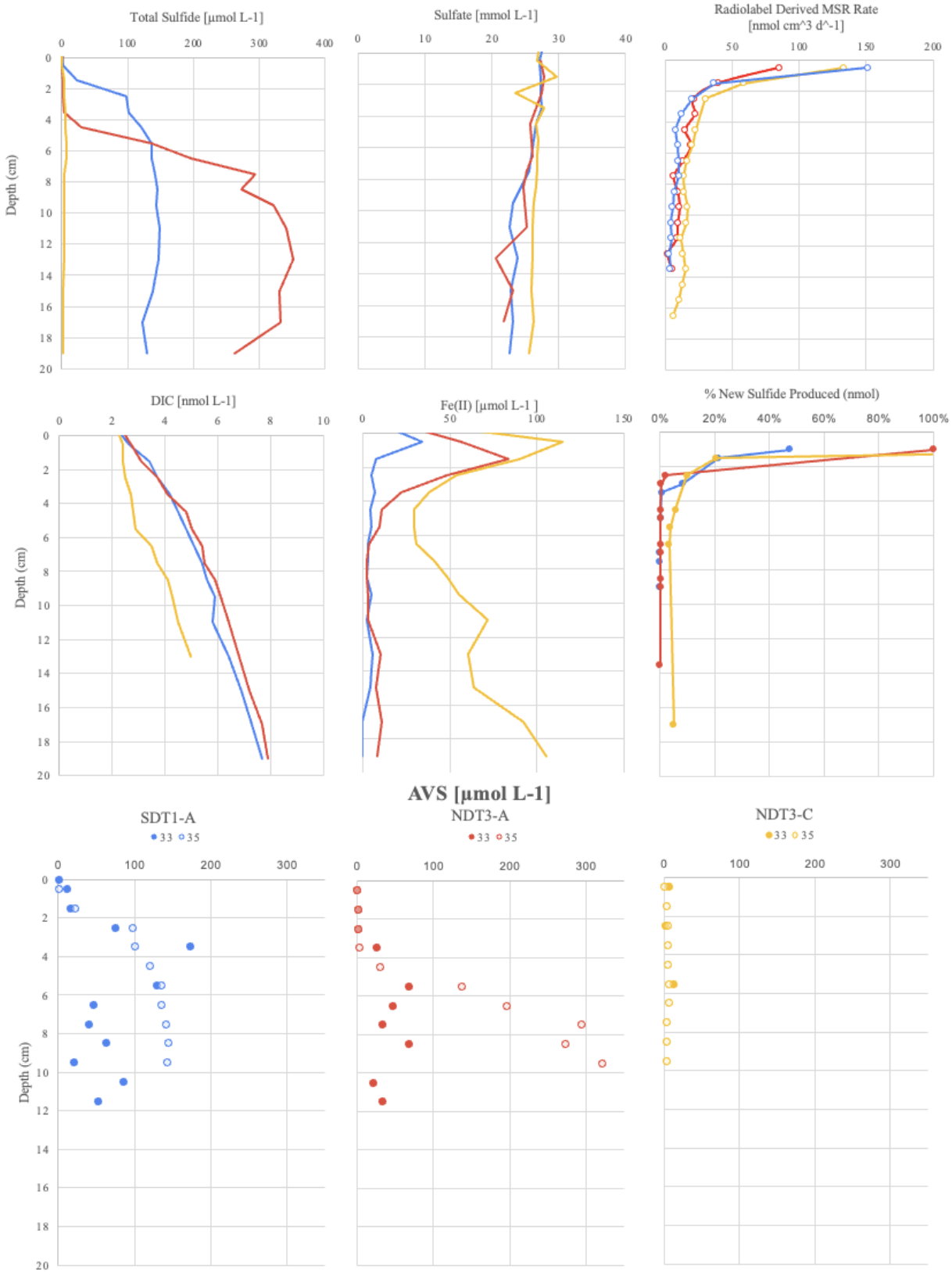

Figure 3.6A-I. Porewater chemistry and radiolabel rates from SBB (Graphs A-F: De'Marcus Robinson and David J. Yousavich, unpublished data). All cores are color coordinated to the same color scheme for each graph, SDT1-A (blue), NDT3-A (red), and NDT3-C (yellow). Top three panels display pore water total concentrations for **A.** sulfide (µM), **B.** sulfate (mM), **C.** MSR rate from radiotracer SRR (nmol*cm^{-3}*d^{-1}), **D.** DIC (mM), E.) Fe^{2+} (µM), **F.** Percent new sulfides produced during incubation period (nmol) from radiotracer cores **G-I.** total AVS sulfides (uM) recovered in parallel SDT1-A, NDT3-A, and NDT3-C. Radiolabel data was processed by Truede Lab at UCLA. Calculated amount of new sulfide created during the incubation period based on radiolabel rates.

All cores were collected below the western sill of the basin (475 m) to examine rates at varying water depths (Fig 3.7). Pore water sulfate (Fig 3.6B) reflects standard oceanic concentrations of 29.66 mM to 20.58 mM. Dissolved inorganic carbon (Fig 3.6D), gradually accumulates with core depth beginning at 1.9 mM at the surface and increasing to 7.9 mM at 19 cm in all three cores. Reactive iron is highest at 0.5 cm for all three cores, with a maximum of 114.5 mM in NDT3-A and then sharply decreases in concentration from 2-4cm, dropping to of 0-2.2 µM for NDT1-A and SDT1-A, for core NDT3-C, iron begins to accumulate again after 4.5 cm reaching 105.2 µM at 19 cm.

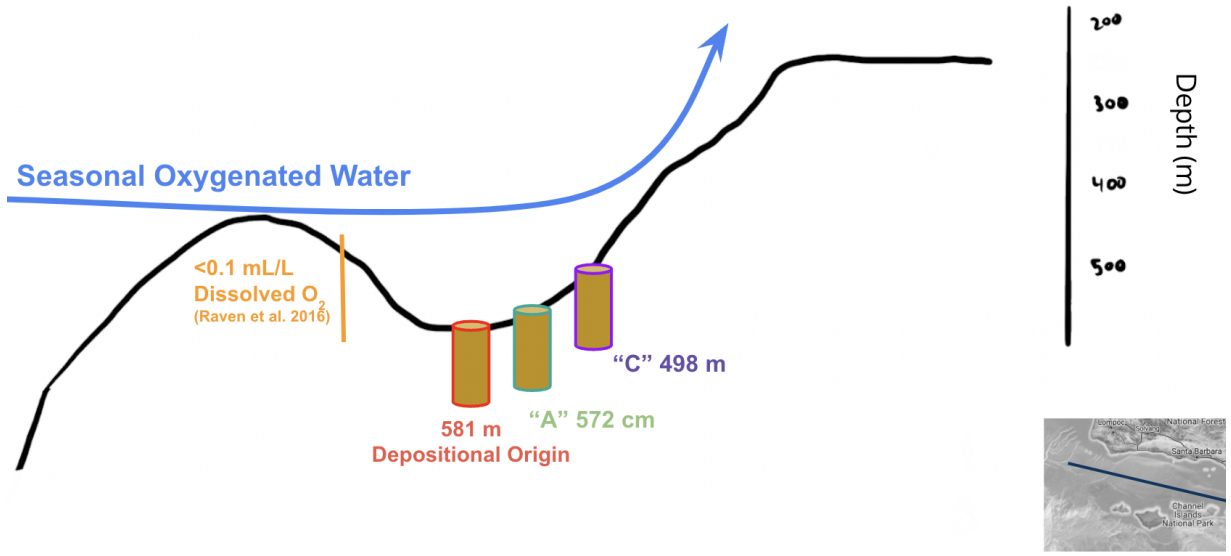

Figure 3.7. Sketch of coring heights in bathymetry of SB viewing E-W. Western sill of the basin (475 m) (secondary rightmost mound). The transept inlet picture is not to the exact scale. Bottom water oxygen is <0.1 mL/L; <10 lM O_2) except during spring inflow events (Goricke 2015).

Total accumulated sulfide as AVS from an unlabeled core (Fig 3.6A) is lowest within the top 6.5 cm, ranging from 6-100 μM. After 6.5cm, accumulated sulfide increases dramatically and remains at that concentration for the remainder of the 6.5-16cm of the sediment core. The maximum concentration of accumulated sulfides is different for each core. Two cores, NDT3-A and SDT1-A were both sampled at 572 cm water from different coordinate locations (Table 3.1). NDT3-A has sulfide accumulation which begins to gradually accumulate from 0.5-3.5 reaching 100 μM at 3.5cm and remaining constant at 100 μM-140 μM from 4.5-9.5 cm. At the same water depth, but a different location (Table 3.1), core SDT1-A finishes accumulating sulfide at 6.5, then gradually maxing out at 350 μM at 9.5 cm then begins to slightly decrease to 250 μM at 18 cm. NDT3-C, which was sampled at the shallowest water depth of the three cores, 498m, shows less than 30 μM sulfide throughout the entire core. NDT3-C has the second highest rate of SRR (Fig 3.6C) at 133.71 $nmol*cm^{-1}*day^{-1}$. This most likely means that the sulfides are reoxidizing or diffusing out of the sediment. This case demonstrates the importance of gross vs. net sulfide production in terms of the overall sedimentary sulfur cycle as interpreting just the pore water chemistry gives the illusion that site NDT3-C does not have an active sulfate reducing population which is found to be the opposite case when SRR are measured.

Sulfide preservation in cores containing the 33-S label were consistently lower in total AVS concentrations than 35-S (Fig 3.6C). This may be due to oxidation during storage. Samples from $^{33}S\text{-}SO_4^{2-}$ cores were immediately frozen following the incubation period and stored at -20°C for three years before AVS extraction. Whereas 35-S was collected and quantified aboard the research vessel within 72 hours of core sampling. Future studies should consider processing AVS fractions from the 33-S cores shortly after collection to avoid sulfide loss with time.

Model $\delta^{34}S$ and $\Delta^{33}S$ SBB Data

This study does not include isotopic data from the 33-S cores, however existing porewater data from unlabeled cores and radiotracer rates were used to model what the $\delta^{34}S$ and $\Delta^{33}S$ signatures should be when isotope data for the ^{33}S can be processed. The calculations behind this model are listed in Section 1.1 in the introduction, specifically Table 1.4, and a table format of the exact calculator used to estimate $\delta^{34}S$ and $\Delta^{33}S$ is listed in the supplemental section as Table 5.2. For each 1 cm segment of sediment, the measured total sulfate concentration and pore water volume were varied using real core and porewater chemistry data measured by De'Marcus Robinson and David J. Yousavich. Epsilon values, and $d^{34}S$ values were varied for three segments of depth, 0-3.5cm, 4.5-10.5, and 10.5-20cm using an average of values cited from previous SBB studies (Raven et al. 2016, Brüchert et al., 1995, and Kaplan et al. 1963). Depth segments were grouped by similar trends in $\delta^{34}S$-H_2S values from Raven et al. (2016) and Brüchert et al., (1995).

Table. 3.3 Isotopic inputs from literature values previously published for 0-20cm of SBB sediments: Raven et al. (2016), Brüchert et al., (1995), and Kaplan et al. (1963). Epsilon values used in the 33-S model to calculate the amount of 33-S labeled sulfide were calculated using equation 2 from $\delta^{34}S$-H_2S and $\delta^{34}S$-SO_4^{2-} observed by Raven et al. (2016) and Brüchert et al., (1995).

Depth	**ε_{MSR}**	**$\delta^{34}S$-SO_4^{2-}**	**$\delta^{34}S$-H_2S**
0.5-3.5 cm	27.25‰	21.5	-3.3
4.5-10.5 cm	41.2‰	22.03	-13.81
10.5-20 cm	23.1‰	22.33	-2.88

The mixed initial sulfur isotope distribution was calculated based on Eq. 2a and 2b which represents the isotope distribution of the initial concentration of SO_4^{2-} in the pore water and the amount of ^{33}S which was spiked into the core (Table 3.3). The amount of new sulfides produced during the incubation period were then calculated using ε_{MSR} values from Raven et al. (2016) and Brüchert et al., (1995) (Table 3.3). The isotope distribution of the new sulfide and $\Delta^{33}S$ was then

mixed back into existing accumulated sulfide isotope compositions using literature values from Raven et al. (2016) and Brüchert et al., (1995). Below, Fig. 3.8, plots $\delta^{34}S$ associated with the newly formed sulfides. The right-hand panel plots expected $\Delta^{33}S$ with depth.

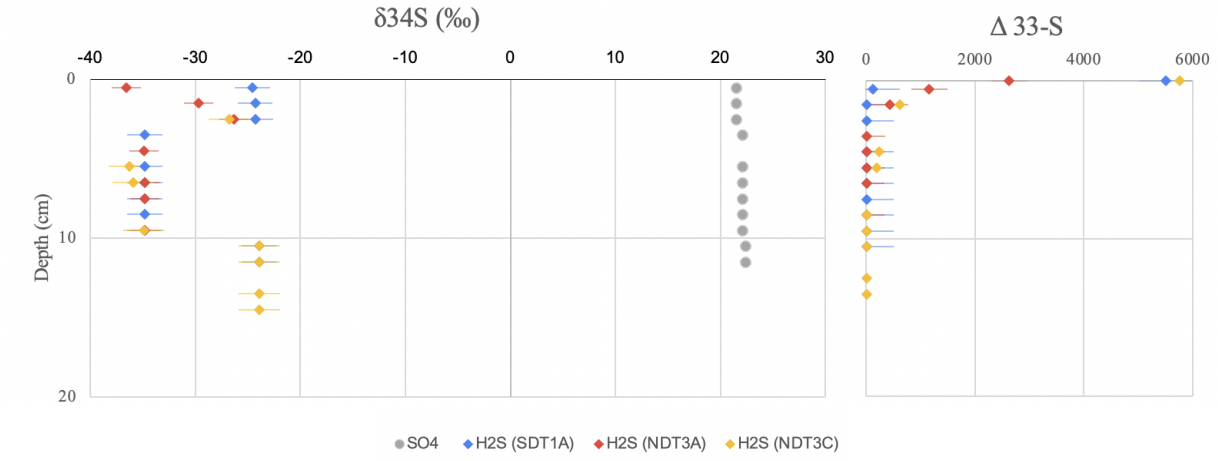

Figure 3.8 Modeled newly formed $\delta^{34}S$-H_2S and estimated $\Delta^{33}S$ Values for SBB Sediments. $\delta^{34}S$-H_2S values with standard error bars calculated for SDT1-A, NDT3-A, NDT3-C. Sulfate and epsilon values used as inputs for the 33-S model were cited from Raven *et al.* (2016), Brüchert *et al.,* (1995), and Kaplan *et al*. (1963). Gray dots are an average $\delta^{34}S$-SO_4^{2-} values published by Raven *et al.* (2016). **LEFT:** Estimated $\Delta^{33}S$ values for core sites SDT1A, NDT3A, NDT3C.

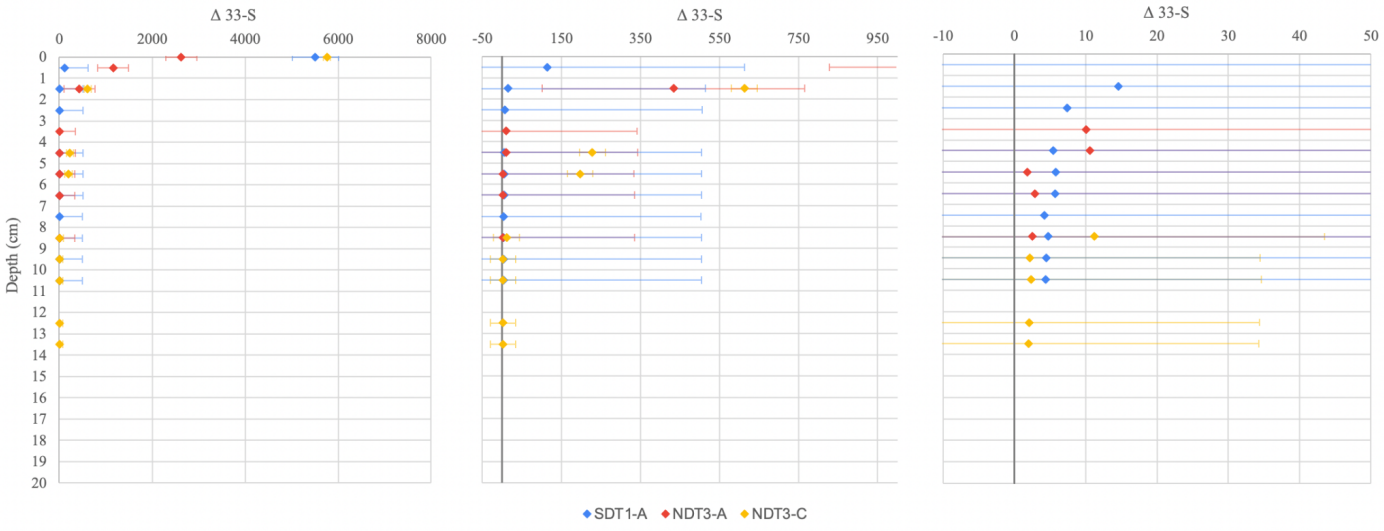

Figure 3.9 Estimated $\Delta^{33}S$ values with increasingly scaled x-axis. All three panels replicate the same data. The left panel is the full range of calculated $\Delta^{33}S$ from 0-8000‰. The center panel is $\Delta^{33}S$ from 0-1000‰. The right panel is $\Delta^{33}S$ from 0-50‰. Blue dots indicate SDT1-A core, red indicates NDT3-A core, and yellow indicates NDT3-C. Error bars are calculated from MSR rate uncertainty.

The estimated $\Delta^{33}S$ values associated with newly formed 33-S labeled sulfides are largest within the top 0.5cm, ranging from 2626‰ to 5757‰ (Figure 3.9). Then exponentially drop off from 0.5-3.5 cm for all cores, settling at an $\Delta^{33}S$ of 2.01‰ to 11.19‰ for all cores 4.5 cm and deeper (Figure 3.9). For context if an epsilon value of 34‰ and zero percent of the new sulfide is labeled the calculated $\delta^{33}S$ is 10.76‰. This trend aligns with the SRR measured by the radiotracer. Large $\Delta^{33}S$ values are a result of fast SRR which produce the most amount of sulfide within the incubation period. Then as SRR slows down the core, less labeled sulfide is produced producing small $\Delta^{33}S$ values.

To demonstrate the linear relationship of $\Delta^{33}S$ values and sulfur reduction rate, (Figure 3.10) plots calculated $\Delta^{33}S$ values by the amount of newly formed labeled sulfide (percent labeled AVS) using a broad range of epsilon values. Varying epsilon values do not impact the $\Delta^{33}S$ values significantly meaning the tracer. However, even when 1% of newly produced sulfide is labeled the minimum $\Delta^{33}S$ calculated for all epsilon inputs was 63.6 ±0.8‰ which is still distinguishably greater than the background value which is $\Delta^{33}S$ =0. The minimum detection limit is equivalent to a mixing ratio of 0.01%, or 100 ppm which produces $\Delta^{33}S$ of 0.63 ±0.008‰. Additionally, $\Delta^{33}S$ are not sensitive to epsilon values (Fig 3.10). The lowest estimated $\Delta^{33}S$ value for this study is 1.77‰ at 6.5 cm in core NDT3-A which is still above the minimum detection limit of $\Delta^{33}S$= 0.63 ±0.008‰, however the sensitivity of the tracer decreases as SRR drops below less than 1% per day from 2.5-11.5cm in SDT1-A, 4.5-9.5cm in NDT3-A, and 7.5-14.5 cm for NDT3-C. In conclusion, the use of 33-S is not recommended in environments where less than 0.1% of sulfide is produced in a day.

Figure 3.10 Sensitivity of $\Delta^{33}S$ with amount of new sulfides produced. To calculate this, 2mL of seawater at $d^{34}S$=21‰ was used. Each line represents a different epsilon value.

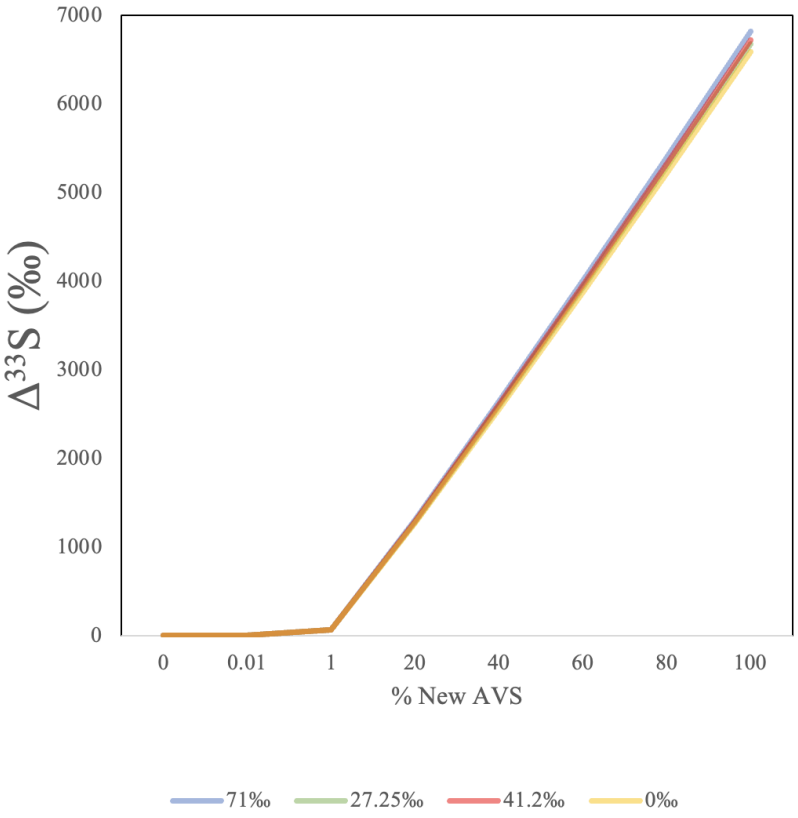

Similarities Between Labeled $\delta^{34}S$-H_2S and Observed $\delta^{34}S$-Py

Sedimentary pyrite represents a dominant sink for marine sulfur (Jorgensen 2019). Liu *et al.,* (2020) demonstrated bulk pyrite isotopes may depend on whether the pyrite formed near the sediment surface or at depth in the sediment column, sedimentation rates, and proximity to sulfate-methane transition zones (Liu *et al.,* 2020; Meister *et al.,* 2019). In SBB sediments, the rate of pyrite formation is generally highest in the top ten centimeters of where there is the most availability of reducible iron (Reimers et al., 1996; Raven et al., 2016, Abdulla et al. 2020). Thus $\delta^{34}S$ values of pyrite should directly reflect the integrated $\delta^{34}S$ of sulfides produced immediately following MSR. However, $\delta^{34}S$ values between accumulated sulfides and pyrite (Raven et al. 2016) indicate a large gap, creating uncertainty in whether $\delta^{34}S$-Py values accurately capture and

preserve $\delta^{34}S$ values created by MSR alone, which may alter current interpretations of $\delta^{34}S$-Py as a paleoclimate proxy for microbial life on the seafloor.

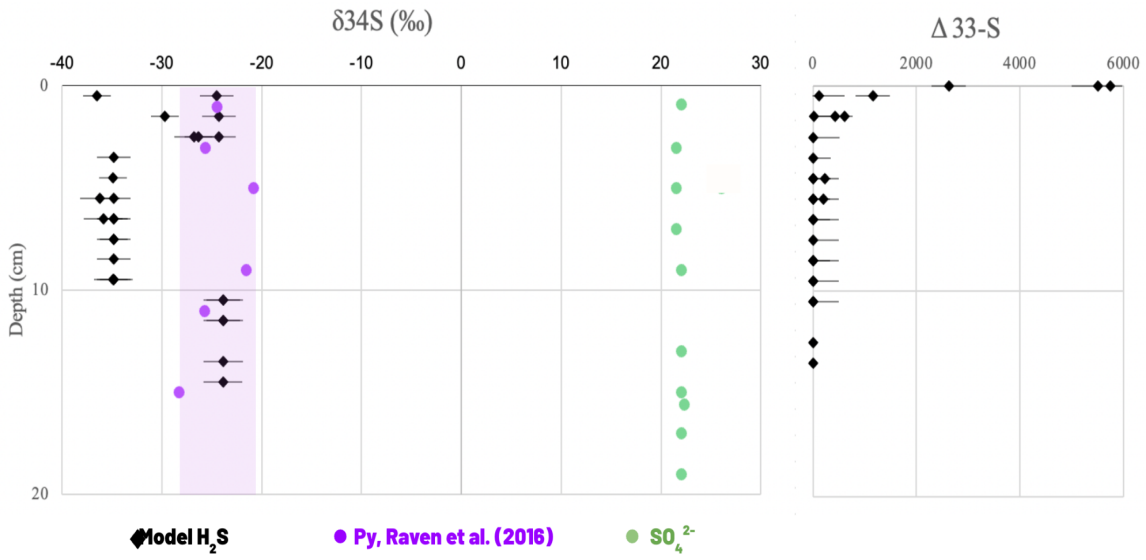

Figure 3.11 Predicted $\delta^{34}S$ values and $\Delta^{33}S$ for AVS in SBB. LEFT PANEL: All colored dots are $\delta^{34}S$ values measured in Santa Barbara sediments from Raven *et al.* (2016), Brüchert *et al.*, (1995), and Kaplan *et al.* (1963). Green dots indicate $\delta^{34}S$-SO_4^{2-}, purple dots: $\delta^{34}S$-Pyrite. Black diamonds are calculated $\delta^{34}S$-H_2S. Estimated $\delta^{34}S$-H_2S were calculated using sediment densities from NDT3A, NDT3C, and SDT1A cores, and estimated % new sulfide from 35 rates measured in parallel cores. Sulfate and epsilon values used in the 33-S model were cited from Raven *et al.* (2016), Brüchert *et al.,* (1995), and Kaplan *et al*. (1963), values were varied based on depth intervals specified in Table 3.3. **LEFT PANEL: Estimated $\Delta^{33}S$ for AVS in SBB**, same as left panel in figure 3.7.

To explore this gap, $\delta^{34}S$-H_2S_{label} values were modeled based on the percent labeled AVS measured by the parallel radiotracer cores (Figure 3.11). Labeled sulfides produced within the incubation period which are ≤8 hours old and thus $\delta^{34}S$ should reflect fractionations produced solely during MSR prior to any further abiotic or biotic processes. Because of this, oxidation of labeled sulfides during the incubation period is likely minimal due to the short incubation time.

However, actual δ^{34}S-AVS values are expected to lean slightly heavier than model values to account for the fact that oxidative processes have a slight isotopic preference for the lighter isotope. These processes may still occur during the incubation, but should remain distinguishably lighter relative to accumulated sulfides.

The largest expected $\delta^{34}S\text{-}H_2S_{label}$ are estimated to range between -50.1‰ and -24.3‰ occurring where SRR are the fastest. These values overlap with the δ^{34}S values observed for pyrites found at 0-3.5 cm which have an average $\delta^{34}S=28\pm4$‰ (Raven *et al.* 2016). This overlap in calculated sulfide and observed pyrite δ^{34}S values (Raven *et al.* 2016, Brüchert *et al.,* 1995). From depths 9.5 cm to 16.5 cm, the expected Δ^{33}S values are less than 3‰ at these depths meaning roughly less than 1% of AVS is labeled thereby modeled δ^{34}S values are more representative of the background δ^{34}S composition of accumulated sulfides (Raven *et al.* 2016, Brüchert *et al.,* 1995) in which the $\delta^{34}S\text{-}H_2S_{label}$ was unmixed as very little new sulfides were produced, decreasing the sensitivity of $^{33}S\text{-}SO_4^{2-}$ calculation. The depths from this experiment which are expected to have a resolvable ^{33}S rate are where SRR are above 1% per day from 0.5-1.5cm in SDT1-A, 0.5-3.5cm in NDT3-A, and 0.5-6.5 cm in NDT3-C.

3.3 Chapter Conclusion

The second foundational step in establishing the $^{33}SO_4^{2-}$ method was to conduct parallel whole-core incubations in experiments in a natural SRB population. The fastest rates and thereby largest estimated Δ^{33}S values were observed within the top 3.5 cm for all 33-S cores which correspond to the trends observed by radiotracer rates with depth. Predicted Δ^{33}S values vary primarily as a result of differences in MSR rate, which exponentially decreases with depth (Fig.3.8). Accordingly, predicted Δ^{33}S values for the mixture of initial and new sulfide in pore water also exponentially

decrease from 0.5-3.5 cm for all cores and level off at 2.01‰ to 11.19‰ with a standard error of 0.75‰ for 4.5-16.5 cm.

Predicted $\delta^{34}S\text{-}H_2S_{label}$ were calculated by subtracting epsilon-MSR values from (Raven *et al.* 2016, Brüchert *et al.,* 1995) from known pore water sulfate $\delta^{34}S$ values (Raven *et al.* 2016, Brüchert *et al.,* 1995), yielding values ranging between -50.1 and -24.3‰ with a standard error of 2.84‰ between 0.5-10.5 cm. Calculated values represent estimated $\delta^{34}S\text{-}H_2S$ values for AVS fraction recovered in 33-S cores, and they overlap with the $\delta^{34}S$ values observed for pyrites found at 0-3.5 cm which have an average $\delta^{34}S$=28±4‰ (Raven *et al.* 2016). From depths 9.5 cm to 16.5 cm, the $\Delta^{33}S$ values are less than 3‰ at these depths meaning roughly less than 1% of AVS is labeled thereby modeled $\delta^{34}S$ values are more representative of the background $\delta^{34}S$ composition of accumulated sulfides (Raven *et al.* 2016, Brüchert *et al.,* 1995) in which the $\delta^{34}S\text{-}H_2S_{label}$ was unmixed as very little new sulfides were produced, decreasing the sensitivity of $^{33}S\text{-}SO_4^{2-}$ calculation. The minimum detection limit for ^{33}S is equivalent to a mixing ratio of 0.01%, or 100 ppm which produces $\Delta^{33}S$ of 0.63 ±0.008‰. The use of $^{33}SO_4^{2-}$ is better suited in environments where over 1% of new sulfides are produced during a 24 hours or with an accumulated sulfide pool less than 100 ppm. Examples of environments which fit these qualifications are the first 3.5-7.5 cm of anoxic surface sediments, or sites where MSR is occurring rapidly and in large volumes with a small accumulated sulfide pool such as microbial matts or sinking particles.

Chapter 4. General Discussion

The development of a ^{33}S-sulfate tracer method is motivated by an interest in creating a minimally disruptive method to measure SRR and stable S-isotope distributions jointly in studies that demand in-situ experiments and radioactivity-free logistics. Furthermore, recovering isotope fractionations produced by complex microbial populations in real environments over the course of a few hours provides a fresh perspective of how sulfide is transformed post-MSR, which directly informs interpretations of modern and paleo-environmental records.

Requirements of Stable Tracer

Preparation and execution of incubation experiments using either tracer methods is relatively identical, varying only in the final stages at the data retrieval stage (Table 4.1). The radioactivity of the radiotracer in each fraction is measured using scintillation and thus the only post incubation step is to extract AVS. Initial and final concentrations of pore water species can be measured directly in scintillation fluid, and extracted AVS solids can also be directly diluted in scintillation fluid and measured as a solid suspension forgoing oxidation. Scintillation is a relatively straight-forward method, requiring less than 5 minutes of counting time per sample, with little to no maintenance on the instrument itself. As for $^{33}SO_4^{2-}$, AVS is required post incubation, and extracted sulfides must be oxidized, purified using strong anion-exchange resin, and uniformly concentration matched before isotope distributions can be measured on an ICP-MS. Additionally, in order to retrieve epsilon-MSR fractionation factors in addition to rates, information about the background signature of $\delta^{34}S\text{-}H_2S$ and $\delta^{34}S\text{-}SO_4^{2-}$ is required for unmixing calculations. Therefore a secondary core without tracer is measured for natural abundance data $\delta^{34}S\text{-}H_2S$ and $\delta^{34}S\text{-}SO_4^{2-}$ is recommended. Additional pieces of geochemical data include the starting concentration of SO_4^{2-}

and the amount of porewater per segment of sediment. Overall, using $^{33}SO_4^{2-}$ is more data intensive than $^{35}SO_4^{2-}$.

Table 4.1 Comparison of radiotracer tracer and stable minor isotope tracer methods and the information retrieved by each respective method.

	Radioactive Tracer ($^{35}SO_4^{2-}$)	**Stable Minor Isotope Tracer ($^{33}SO_4^{2-}$)**
Preparation of Tracer	Oxidation of ^{35}S Standard Using CRS	Oxidation of ^{33}S Standard Using CRS
Methodology in Field	Whole Core Incubation	Whole Core Incubation
Fractions Retrieved Containing Tracer	Pore Water Sulfates Porewater Sulfides AVS	Pore Water Sulfates Porewater Sulfides AVS
Type of Analytical Tool	Scintillation	MC-ICP-MS
Information Recovered	MSR Rate	MSR Rate ($\delta^{33}S$) $\delta^{34}S \rightarrow \varepsilon_{msr}$

Sensitivities of $^{33}SO_4^{2-}$ Tracer

A strong effect on isotope unmixing that affects both 35-S and 33-S is caused by a concurrent reoxidation of the formed labeled sulfide back to labeled sulfate during the incubation experiment. This may be remedied by shorter incubations, as with prolonged incubation time providing more opportunities for sulfate reduction rate to equal that of sulfide oxidation rate lowering net SRR (Fossing, 1995). The effect of sulfide reoxidation is thought to be largest at the surface where there is a very small free sulfide pool (Jorgensen 2021) (Figure 3.6A). The re-oxidation is a long-standing hole in sulfur mass-balances modeling of pore water sulfate; however, the comparison of newly formed $\delta^{34}S$ to accumulated $\delta^{34}S$ signatures and $\delta^{34}S$-Py signatures may help to bridge this gap as if $\delta^{34}S$ values of labeled AVS reflect $\delta^{34}S$ values captured in pyrite, as if newly produced sulfide $\delta^{34}S$ values do not resemble $\delta^{34}S$ pyrite values this would imply that additional fractionations from oxidation and/or microbial disproportionation have occurred.

Future Applications

The logistics of using radiotracers in real life environments is continually becoming more limited. The use of radioactive substances comes with limitations on travel to field sites both domestically and internationally. Additionally, incubations *in situ* using a radioactive substance are almost never an option. Sediment cores or pore water samples must be removed from the sampling site to avoid injected a radioactive substance into the environment. This causes disruptions to natural microbial activities and potential loss of the population density through changes in temperature and pressure, accidental oxygenation, loss of sulfides, contamination of surface sediments (Røy *et al.*, 2014). Using a stable isotope which can be used *in situ* is a valuable option for examining minimally disturbed microbial populations.

In addition to tracking 33-S from sulfate to sulfide, 33-S can be used to track the speciation of organic sulfur and other reduced sulfur pools such as FeS, polysulfides, organic sulfur, and SO_4^{2-} which can form through series of rapidly occurring biogeochemical processes which can be tedious if not impossible to detect analytically (Fossing and Jørgensen, 1990). Additionally, measuring $^{33}SO_4^{2-}$ with NanoSIMS introduces a way to track transformations in sulfur isotope compositions spatially on a micron-scale to understand the local variability of microbial metabolic activity. With these future applications in mind, the use of $^{33}S\text{-}SO_4^{2-}$ to measure SRR and ε_{msr} concurrently is potentially a powerful new tool for investigating active sites of MSR to learn how sulfur moves throughout interfacial environments which are the targets of larger biogeochemical questions and ongoing carbon storage research.

Conclusion

There is a disconnect in our current understanding of how sulfur isotopes are deposited in the sediment record as no technique exists to study MSR rates and fractionation jointly. This study

lays the framework for the use of $^{33}SO_4^{2-}$ to track the movement of ^{33}S labeled sulfate to ^{33}S labeled sulfide to be used *in situ* to simultaneously measure sulfur reduction rates and fractionations. To establish this methodology, $^{33}SO_4^{2-}$ was directly compared to the rates captured by well established radiotracer $^{35}SO_4^{2-}$ in a pure culture incubation and a whole core incubation.

In the first half of this study, parallel incubations of ^{33}S-SO_4^{2-} and well established ^{35}S-SO_4^{2-} using pure culture *Desulfovibrio vulgaris Hildenborough* (DvH) were used to compare SRR captured by both $^{35}SO_4^{2-}$ and $^{33}SO_4^{2-}$. The growth rate of DvH was 0.12 hr^{-1} with a doubling time of 5.6 min which reflected literature values (Ramel *et al.* (2015), Johnson *et al.* (1997), Mukhopadhyay (2006), Borglin *et al.* (2008). However, there is likely an issue with the media limiting cell growth as the maximum OD reached was 0.12 whereas literature values observed a max OD of 0.89-1.00 (Ramel *et al.* 2015, Johnson *et al.* 1997, Mukhopadhyay 2006, Borglin *et al.* 2008). Because these values are scattered on either side of the 1-1 line, they demonstrate no clear bias for either label, but these results are inconclusive as to whether there is difference in uptake by either label during MSR. To improve precision on SRR values for both tracers additional repetitions of the experiment and swipe-tests for 35-S cross contamination will be required. The results of the pure culture incubations provide a preliminary argument for the interchangeable uptake of $^{35}SO_4^{2-}$ and $^{33}SO_4^{2-}$ by sulfate reducing organisms to measure SRR. This may become a valuable alternative in situations where the radiotracer cannot be used.

The second foundational step in establishing the $^{33}SO_4^{2-}$ method was to conduct parallel whole-core incubations in experiments in a natural SRB population in parallel sub-oxic Santa Barbara Basin (SBB). Using radiolabeled rates from the parallel radiolabel core, and sulfate and epsilon values cited from Raven et al. (2016), Brüchert et al., (1995), and Kaplan et al. (1963) $\Delta^{33}S$ values and $\delta^{34}S$-H_2S_{label} were estimated for three ^{33}S cores. Paralleling MSR rates from 35S, the

largest estimated $\Delta^{33}S$ values were calculated for the top 3.5 cm for all 33-S cores, below which values exponentially decrease from 0.5-3.5 cm for all cores and level off at 2.01‰ to 11.19‰ for 4.5-16.5 cm. From depths 9.5 cm to 16.5 cm, the $\Delta^{33}S$ values are less than 3‰ at these depths meaning roughly less than 1% of AVS is labeled thereby modeled $\delta^{34}S$ values are more representative of the background $\delta^{34}S$ composition of accumulated sulfides (Raven *et al.* 2016, Brüchert *et al.,* 1995). The minimum detection limit is equivalent to a mixing ratio of 0.01% between newly formed and background (pre-existing) sulfides, or 100 ppm which produces $\Delta^{33}S$ of 0.63 ±0.01‰ regardless of ε_{MSR}. The lowest estimated $\Delta^{33}S$ value for this study is 1.77‰ at 6.5 cm in core NDT3-A which is still above the minimum detection limit of $\Delta^{33}S$= 0.63‰, however the sensitivity of the tracer decreases as SRR drops below less than 1% per day. Because of this, the use of $^{33}SO_4^{2-}$ is not appropriate in systems which overturn at less than 1% new sulfides a day.

The use of ^{33}S-SO_4^{2-} to measure SRR and ε_{msr} jointly could provide a powerful tool for quantifying cryptic sulfur reduction processes. These two studies demonstrated the potential for $^{33}SO_4^{2-}$ to be used for *in situ* experiments in environments where MSR is occurring rapidly and in large magnitudes. The conclusions of these two studies pave the way for the eventual use of $^{33}SO_4^{2-}$ to be used to assist research surrounding cryptic sulfur cycling.

Works Cited

Abdulla, Burdige, D. J., & Komada, T. (2020). Abiotic formation of dissolved organic sulfur in anoxic sediments of Santa Barbara Basin. Organic Geochemistry, 139, 103879–. https://doi.org/10.1016/j.orggeochem.2019.05.009

Behl, Richard & Escobedo, D. & Kennett, J. & Nicholson, Craig & Sorlien, Christopher. (2007). Decadal to Million-Year Sedimentation Rates and the Ultra-High-Resolution Marine Record From Santa Barbara Basin. AGU Fall Meeting Abstracts.

Bernhard, J.M., Reimers, C.E. (1991). Benthic foraminiferal population fluctuations related to anoxia: Santa Barbara Basin. Biogeochemistry 15, 127–149. https://doi.org/10.1007/BF00003221

Bertran, E., Leavitt, W. D., Pellerin, A., Zane, G. M., Wall, J. D., Halevy, I., Wing, B. A., & Johnston, D. T. (2018). Deconstructing the Dissimilatory Sulfate Reduction Pathway: Isotope Fractionation of a Mutant Unable of Growth on Sulfate. Frontiers in microbiology, 9, 3110. https://doi.org/10.3389/fmicb.2018.03110

Borglin, Joyner, D., Jacobsen, J., Mukhopadhyay, A., & Hazen, T. C. (2008). Overcoming the anaerobic hurdle in phenotypic microarrays: Generation and visualization of growth curve data for Desulfovibrio vulgaris Hildenborough. Journal of Microbiological Methods, 76(2), 159–168. https://doi.org/10.1016/j.mimet.2008.10.003

Brüchert, Pratt, L. M., Anderson, T. F., & Hoffmann, S. R. (1995). Abundance and isotopic composition of organic and inorganic sulfur species in laminated and bioturbated sediments from Hole 893A, Santa Barbara Basin: Santa Barbara Basin : covering Leg 146 of the cruises of the Drilling Vessel JOIDES Resolution, Santa Barbara Channel,

California, Site 893, 20 September-22 November 1992. Proceedings of the Ocean Drilling Program. Scientific Results, 146, 219–229.

Chambers, L. A., Trudinger, P. A., Smith, J. W., & Burns, M. S. (1975). Fractionation of sulfur isotopes by continuous cultures of Desulfovibrio desulfuricans. Canadian journal of microbiology, 21(10), 1602–1607. https://doi.org/10.1139/m75-234

Callbeck, C.M., Canfield, D.E., Kuypers, M.M.M., Yilmaz, P., Lavik, G., Thamdrup, B., Schubert, C.J. and Bristow, L.A. (2021), Sulfur cycling in oceanic oxygen minimum zones. Limnol Oceanogr, 66: 2360-2392. https://doi.org/10.1002/lno.11759

Canfield, D. E. (2001). Biogeochemistry of Sulfur Isotopes. Reviews in Mineralogy and Geochemistry; 43 (1): 607–636. DOI: https://doi.org/10.2138/gsrmg.43.1.607

Canfield, D., & Raiswell, R. (1999). The evolution of the sulfur cycle. American Journal Of Science, 299(7-9), 697-723.

Canfield, D. E., Raiswell, R., Westrich, J. T., Reaves, C. M., & Berner, R. A. (1986). The use of chromium reduction in the analysis of reduced inorganic sulfur in sediments and shales. Chemical geology, 54(1-2), 149-155.

Canfield, & Teske, A. (1996). Late Proterozoic rise in atmospheric oxygen concentration inferred

from phylogenetic and sulphur-isotope studies. Nature (London), 382(6587), 127–132. https://doi.org/10.1038/382127a0.

Detmers, Brüchert, V., Habicht, K. S., & Kuever, J. (2001). Diversity of Sulfur Isotope Fractionations by Sulfate-Reducing Prokaryotes. Applied and Environmental Microbiology, 67(2), 888–894. https://doi.org/10.1128/AEM.67.2.888-894.2001

Fossing, H., Thode-Andersen, S., & Jørgensen, B. (1992). Sulfur isotope exchange between

35S-labeled inorganic sulfur compounds in anoxic marine sediments. Marine Chemistry, 38(1), 117-132.

Fry, B., Gest, H., & Hayes, J. M. (1988). 34S/32S fractionation in sulfur cycles catalyzed by anaerobic bacteria. Applied and Environmental Microbiology, 54(1), 250–256. https://doi.org/10.1128/aem.54.1.250-256.1988

Fry, Jannasch, H. W., Molyneaux, S. J., Wirsen, C. O., Muramoto, J. A., & King, S. (1991). Stable isotope studies of the carbon, nitrogen and sulfur cycles in the Black Sea and the Cariaco Trench. Deep-Sea Research. Part A. Oceanographic Research Papers, 38, S1003–S1019. https://doi.org/10.1016/S0198-0149(10)80021-4

Fry, B,, Vairavamurthy, Schoonen, M. A. A., & Eglinton, T. I. (1995). Geochemical transformations of sedimentary sulfur (Vol. 612). American Chemical Society. pp. 397–410.

Fry, Gest, H., & Hayes, J. M. (1988). 34S/32S fractionation in sulfur cycles catalyzed by anaerobic bacteria. Applied and Environmental Microbiology, 54(1), 250–256. https://doi.org/10.1128/aem.54.1.250-256.1988

Greeff, O., Glud, R.N., Gundersen, J., Holby, O., Jørgensen, B.B. (1998) A benthic lander for tracer studies in the sea bed: in situ measurements of sulfate reduction. Continental Shelf Research 18, 1581-1594.35S sulfate.

Goericke, R., Bograd, S., & Grundle, D. (2015). Denitrification and flushing of the Santa Barbara Basin bottom waters. Deep Sea Research (Part II, Topical Studies in Oceanography), 112(C), 53-60.

Hayes, J. (2004). An Introduction to Isotopic Calculations. https://www.whoi.edu/cms/files/jhayes/2005/9/IsoCalcs30Sept04_5183.pdf

Hoffmann. (1977). Kinetics and mechanism of oxidation of hydrogen sulfide by hydrogen peroxide in acidic solution. Environmental Science & Technology, 11(1), 61–66. https://doi.org/10.1021/es60124a004

Howarth, R. W., & Jørgensen, B. B. (1984). Formation of 35S-labelled elemental sulfur and pyrite in coastal marine sediments (Limfjorden and Kysing Fjord, Denmark) during short-term 35SO42− reduction measurements. Geochimica et cosmochimica acta, 48(9), 1807-1818.

Ivanov M.V, Rusanov I.I, Pimenov N.V, Bairamov I.T, Yusupov S.K, Savvichev A.S, Lein A.Y, & Sapozhnikov V.V. (2001). Microbial Processes of the Carbon and Sulfur Cycles in Lake Mogilnoe. Microbiology (New York), 70(5), 583–593.

Johnson, Zhulin, I. B., Gapuzan, M. E., & Taylor, B. L. (1997). Oxygen-dependent growth of the obligate anaerobe Desulfovibrio vulgaris Hildenborough. Journal of Bacteriology, 179(17), 5598–5601. https://doi.org/10.1128/jb.179.17.5598-5601.1997

Johnston, Farquhar, J., Habicht, K. S., & Canfield, D. E. (2008). Sulphur isotopes and the search for life: strategies for identifying sulphur metabolisms in the rock record and beyond. Geobiology, 6(5), 425–435. https://doi.org/10.1111/j.1472-4669.2008.00171.x

Johnston, D. (2011). Multiple sulfur isotopes and the evolution of Earth's surface sulfur cycle. Earth-science Reviews, 106(1-2), 161-183.

Jørgensen, B. (1979). A theoretical model of the stable sulfur isotope distribution in marine sediments. Geochimica Et Cosmochimica Acta, 43(3), 363-374.

Jørgensen, B.B., Findlay, A.J.L., Pellerin, A. (2019) The biogeochemical sulfur cycle of marine sediments. Frontiers in Microbiology 10, 849

Jørgensen. (2021). Sulfur Biogeochemical Cycle of Marine Sediments. Geochemical

Perspectives, 145–307. https://doi.org/10.7185/geochempersp.10.2

Kallmeyer, J., Ferdelman, T., Weber, A., Fossing, H., & Jørgensen, B. (2004). A cold chromium distillation procedure for radiolabeled sulfide applied to sulfate reduction measurements. Limnology and Oceanography: Methods, 2(6), 171-180.

Ku, Kay, J., Browne, E., Martini, A. M., Peters, S. C., & Chen, M. D. (2008). Pyritization of iron in tropical coastal sediments: Implications for the development of iron, sulfur, and carbon diagenetic properties, Saint Lucia, Lesser Antilles. Marine Geology, 249(3), 184–205. https://doi.org/10.1016/j.margeo.2007.12.001

Kaplan, Emery, K. ., & Rittenbebg, S. . (1963). The distribution and isotopic abundance of sulphur in recent marine sediments off southern California. Geochimica et Cosmochimica Acta, 27(4), 297,IN1,313–312,IN1,331. https://doi.org/10.1016/0016-7037(63)90074-7

Leavitt, W.D., Halevy, I., Bradley, A.S., Johnston, D.T. (2013) Influence of sulfate reduction rates on the Phanerozoic sulfur isotope record. Proceedings of the National Academy of Sciences of the United States of America 110, 11244-11249.

Leavitt, W. D., Bradley, A. S., Santos, A. A., Pereira, I. A., & Johnston, D. T. (2015). Sulfur Isotope Effects of Dissimilatory Sulfite Reductase. Frontiers in microbiology, 6, 1392. https://doi.org/10.3389/fmicb.2015.01392

Li, Gilhooly, W. P., Zerkle, A. L., Lyons, T. W., Farquhar, J., Werne, J. P., Varela, R., & Scranton,

M. I. (2010). Stable sulfur isotopes in the water column of the Cariaco Basin. Geochimica et Cosmochimica Acta, 74(23), 6764–6778. https://doi.org/10.1016/j.gca.2010.08.020

Liu, J., Pellerin, A., Antler, G., Kasten, S., Findlay, A.J., Dohrmann, I., Røy, H., Turchyn, A.V.,

Jørgensen, B.B. (2020) Early diagenesis of iron and sulfur in Bornholm Basin sediments: the role of near-surface pyrite formation. Geochimica et Cosmochimica Acta 284, 43-60.

Liu, Antler, G., Pellerin, A., Izon, G., Dohrmann, I., Findlay, A. J., Roy, H., Ono, S., Turchyn, A.

V., Kasten, S., & Jorgensen, B. B. (2021). Isotopically “heavy” pyrite in marine sediments due to high sedimentation rates and non-steady-state deposition. Geology (Boulder), 49(7), 816–821. https://doi.org/10.1130/G48415.1

Lyons. (1997). Sulfur isotopic trends and pathways of iron sulfide formation in upper Holocene sediments of the anoxic Black Sea. Geochimica et Cosmochimica Acta, 61(16), 3367–3382. https://doi.org/10.1016/S0016-7037(97)00174-9

Mossmann, Aplin, A. C., Curtis, C. D., & Coleman, M. L. (1991). Geochemistry of inorganic and organic sulphur in organic-rich sediments from the Peru Margin. Geochimica et Cosmochimica Acta, 55(12), 3581–3595. https://doi.org/10.1016/0016-7037(91)90057-C

Mukhopadhyay, Zhili He, Huang, K., Huang, R., Joyner, D. C., Katz, N., Keller, M., Oeller, P., Redding, A., Jun Sun, Wall, J., Jing Wei, Alm, E. J., Zamin Yang, Yen, H.-C., Jizhong Zhou, Keasling, J. D., Arkin, A. P., Baidoo, E. E., … Holman, H.-Y. (2006). Salt Stress in Desulfovibrio vulgaris Hildenborough: an Integrated Genomics Approach. Journal of Bacteriology, 188(11), 4068–4078. https://doi.org/10.1128/JB.01921-05

Meister, P., Brunner, B., Picard, A., Böttcher, M.E., Jørgensen, B.B. (2019) Carbon and sulphur isotopes as tracers of past sub-seafloor microbial activity. Scientific Reports 9, 604.

Mandernack, Lynch, L., Krouse, H. ., & Morgan, M. . (2000). Sulfur cycling in wetland peat of

the New Jersey Pinelands and its effect on stream water chemistry. Geochimica et Cosmochimica Acta, 64(23), 3949–3964. https://doi.org/10.1016/S0016-7037(00)00491-9

Paris, Guillaume et al. “MC-ICP-MS Measurement of δ34S and Δ33S in Small Amounts of Dissolved Sulfate.” Chemical geology 345 (2013): 50–61. Web.

Price, & Casagrande, D. J. (1991). Sulfur distribution and isotopic composition in peats from the Okefenokee Swamp, Georgia and the Everglades, Florida. International Journal of Coal Geology, 17(1), 1–20. https://doi.org/10.1016/0166-5162(91)90002-Z

Ramel, Brasseur, G., Pieulle, L., Valette, O., Hirschler-Réa, A., Fardeau, M. L., & Dolla, A. (2015). Growth of the obligate anaerobe Desulfovibrio vulgaris Hildenborough under continuous low oxygen concentration sparging: impact of the membrane-bound oxygen reductases. PloS One, 10(4), e0123455–e0123455. https://doi.org/10.1371/journal.pone.0123455

Ramel, Amrani, A., Pieulle, L., Lamrabet, O., Voordouw, G., Seddiki, N., Brèthes, D., Company,

M., Dolla, A., & Brasseur, G. (2013). Membrane-bound oxygen reductases of the anaerobic sulfate-reducing Desulfovibrio vulgaris Hildenborough: roles in oxygen defence and electron link with periplasmic hydrogen oxidation. Microbiology (Society for General Microbiology), 159(Pt 12), 2663–2673. https://doi.org/10.1099/mic.0.071282-0

Raven, M., Sessions, A., Fischer, W., & Adkins, J. (2016). Sedimentary pyrite δ34S differs from porewater sulfide in Santa Barbara Basin: Proposed role of organic sulfur. Geochimica Et Cosmochimica Acta, 186(C), 120-134.

Røy, H., Weber, H., Tarpgaard, I., Ferdelman, T., & Jørgensen, B. (2014). Determination of dissimilatory sulfate reduction rates in marine sediment via radioactive 35S tracer. Limnology and Oceanography: Methods, 12(4), 196-211.

Rudnicki, Elderfield, H., & Spiro, B. (2001). Fractionation of sulfur isotopes during bacterial sulfate reduction in deep ocean sediments at elevated temperatures. Geochimica et Cosmochimica Acta, 65(5), 777–789. https://doi.org/10.1016/S0016-7037(00)00579-2

Sim, M., Bosak, T., & Ono, S. (2011). Large Sulfur Isotope Fractionation Does Not Require Disproportionation. Science, 333(6038), 74-77. DOI: 10.1126/science.1205103

Sweeney, & Kaplan, I. . (1980). Stable isotope composition of dissolved sulfate and hydrogen sulfide in the Black Sea. Marine Chemistry, 9(2), 145–152. https://doi.org/10.1016/0304-4203(80)90064-X

Thode, H. G. (1960). Sulphur Isotope Fractionation in Early Diagenesis of Recent Sediments of Northeast Venezuela. AAPG Bulletin, 44. https://doi.org/10.1306/0BDA6248-16BD-11D7-8645000102C1865D

Tostevin, R., Turchyn, A., Farquhar, J., Johnston, D., Eldridge, D., Bishop, J., & Mcilvin, M. (2014). Multiple sulfur isotope constraints on the modern sulfur cycle. Earth and Planetary Science Letters, 396, 14-21.

Trudinger, P.A., Chambers, L.A. (1973) Reversibility of bacterial sulfate reduction and its relevance to isotope fractionation. Geochimica et Cosmochimica Acta 37, 1775-1778.

Wildschut, Lang, R. M., Voordouw, J. K., & Voordouw, G. (2006). Rubredoxin:Oxygen Oxidoreductase Enhances Survival of Desulfovibrio vulgaris Hildenborough under Microaerophilic Conditions. Journal of Bacteriology, 188(17), 6253–6260. https://doi.org/10.1128/JB.00425-06

Wing, B.A., Halevy, I. (2014) Intracellular metabolite levels shape sulfur isotope fractionation during microbial sulfate respiration. Proceedings of the National Academy of Sciences of the United States of America 111, 18116-18125.

Westrich J. T. (1983). The consequences and controls of bacterial sulfate reduction in marine sediments. Ph.D. thesis, Yale Univ.

Werne, Lyons, T. W., Hollander, D. J., Formolo, M. J., & Sinninghe Damsté, J. S. (2003). Reduced sulfur in euxinic sediments of the Cariaco Basin: sulfur isotope constraints on organic sulfur formation. Chemical Geology, 195(1), 159–179. https://doi.org/10.1016/S0009-2541(02)00393-5

Yurkiw, Voordouw, J., & Voordouw, G. (2012). Contribution of rubredoxin:oxygen oxidoreductases and hybrid cluster proteins of Desulfovibrio vulgaris Hildenborough to survival under oxygen and nitrite stress. Environmental Microbiology, 14(10), 2711–2725. https://doi.org/10.1111/j.1462-2920.2012.02859.x

5.0 Supplemental Figures and Tables

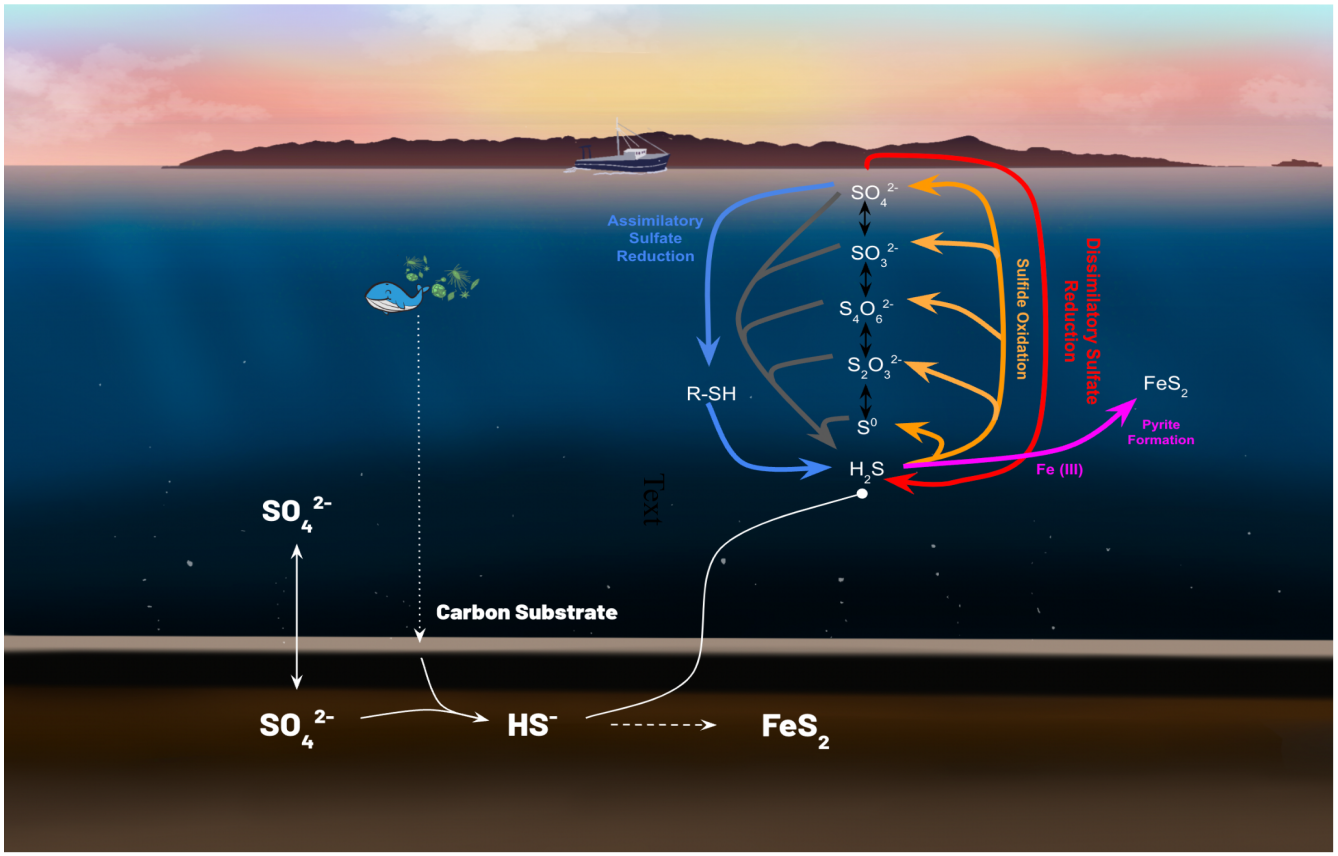

Figure 1.1 Sulfur Cycle Overview in SBB. Representation of sulfur species during sedimentary sulfur cycle in Santa Barbara Basin, California.

Table 5.1 Procedural blanks and standard recoveries for each method used during Chapter 2 and Chapter 3.

Step of Procedure	# of Stds	# of Blanks	Avg Yield Std	% STDEV Std (of % Yield)	Avg Blank (nmol)	STDEV Blanks (nmol)	Standard	Blank	
AVS (minus oxidation blank)	3	3	94.3%	±0.134	1.705	±0.418	ZnS	HCl	
CRS (minus oxidation blank)	3	3	89.8%	±0.298	1.671	±0.404	Elemental S Pyrite	HCl + $CrCl_2$	
Oxidation	[redacted]	3	[redacted]	[redacted]	0.296 (nmol/ mL)	±0.036	[redacted]	H_2O_2	**Percent Cl^- Retained (n = 26)**
Anion-Exchange Resin	17	9	86%	±0.080	-0.0301	±1.0418	Filtered Seawater	IC Dilution Solution (1L MQ+ 200 uL HCl)	0.612%
MQ	[redacted]	5	[redacted]	[redacted]	0.033	±0.038	[redacted]	[redacted]	
IC (200 uL of C* Baseline HCl in 1 L of MQ)	[redacted]	5	[redacted]	[redacted]	0.837	±0.0629	[redacted]	[redacted]	
				SUM of Process	4.5119	±1.5827			

Table 5.2. Example Calculation of Labeled Sulfide modeling and unmixing calculation using trace amount of 33-sulfur label. The lowest relative addition of AVS is set by the precision of the $\Delta^{33}S$ measurement, which is resolvable at 0.31. The *minimum* detection limit is equivalent to a mixing ratio of 0.01%, or 100 ppm.

Sulfate at the beginning of incubation	uM	Vol (mL)	$\delta^{34}S$	$\delta^{33}S$	$\delta^{36}S$	Total/ ^{32}S	µmol ^{34}S	µmol ^{33}S	µmol ^{36}S	µmol ^{32}S
Sea/Pore Water	28000	4	21.0	10.76	40.28	1.04	4.92	0.87	0.02	107.75
Labeled Spike	28000	0.1					0.00	0.00	0.00	0.00
Total							4.92	3.67	0.02	107.75
Estimate Sulfide Production	Epsilon	Mass-Dependence Ratio $^{32}/_{33}$ **(λ)**	α^{34}	α^{33}	α^{36}					
MSR-derived sulfide	-35	0.515	0.965	0.980	0.930					
Mixed Sulfide Pools	%		$\delta^{34}S$	$\delta^{33}S$	**$\Delta^{33}S$**					
Labeled Sulfide	0.01		-14.7	3180.0	3187.6	1.078	0.00	0.00	0.00	0.00
Un-labeled Sulfide	99.99		21.0	10.76	40.28	1.054	0.02	0.00	0.00	0.38
Total After Mixing			**21.0**	**11.07**	**$\Delta^{33}S$ =**	**0.31**	**0.02**	**0.00**	**0.00**	**0.38**

Figure 2.1. Flowchart of method for pure culture incubations. followed for processing bottles containing 33-sulfur and 35-sulfur labels for pure culture incubation experiments.

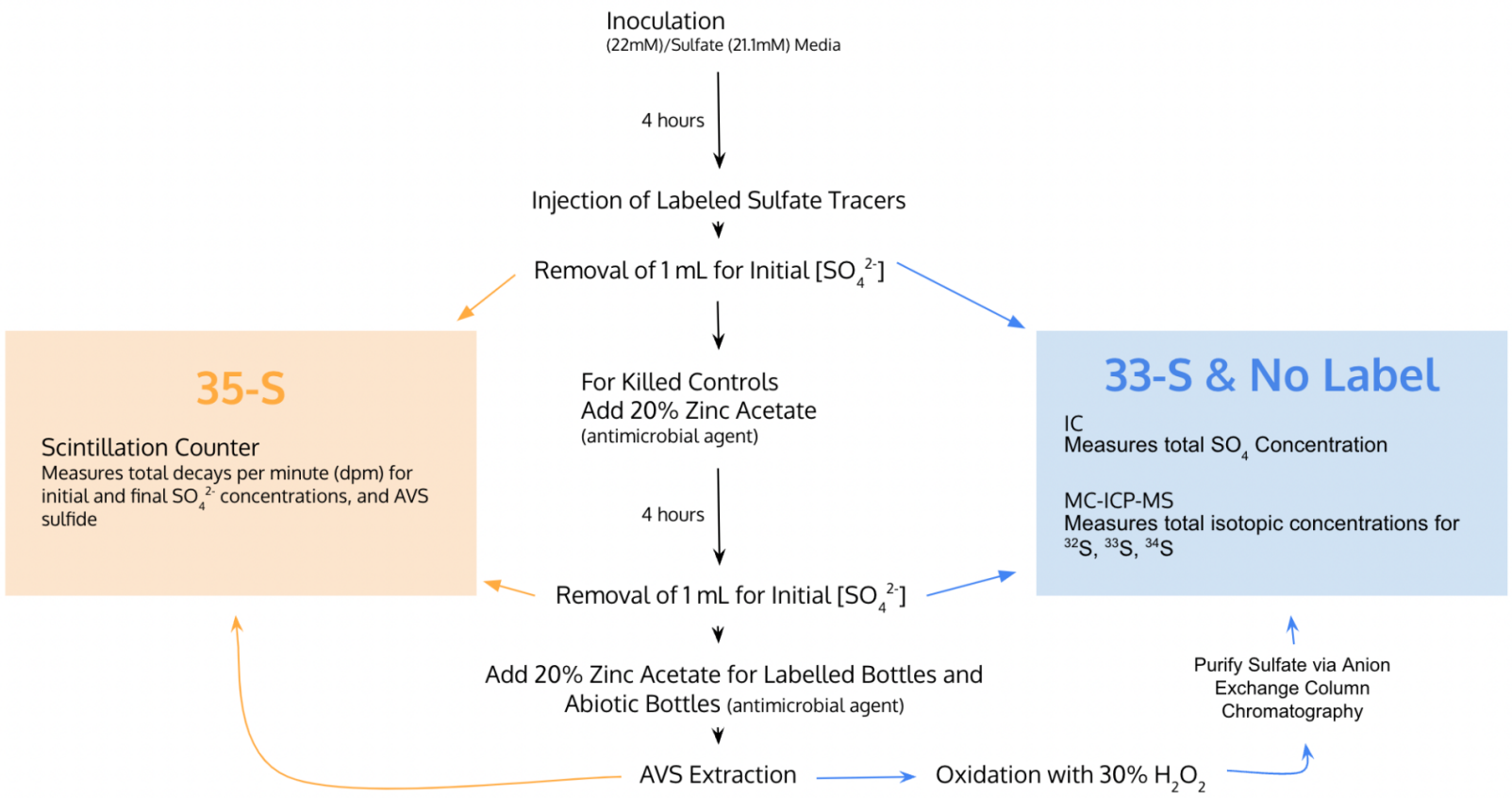

Figure 3.4. AVS and CRS reflux system and zinc acetate trap. Typically six identical set ups are linked to one "line" so that six samples can be sequentially extracted at a time.

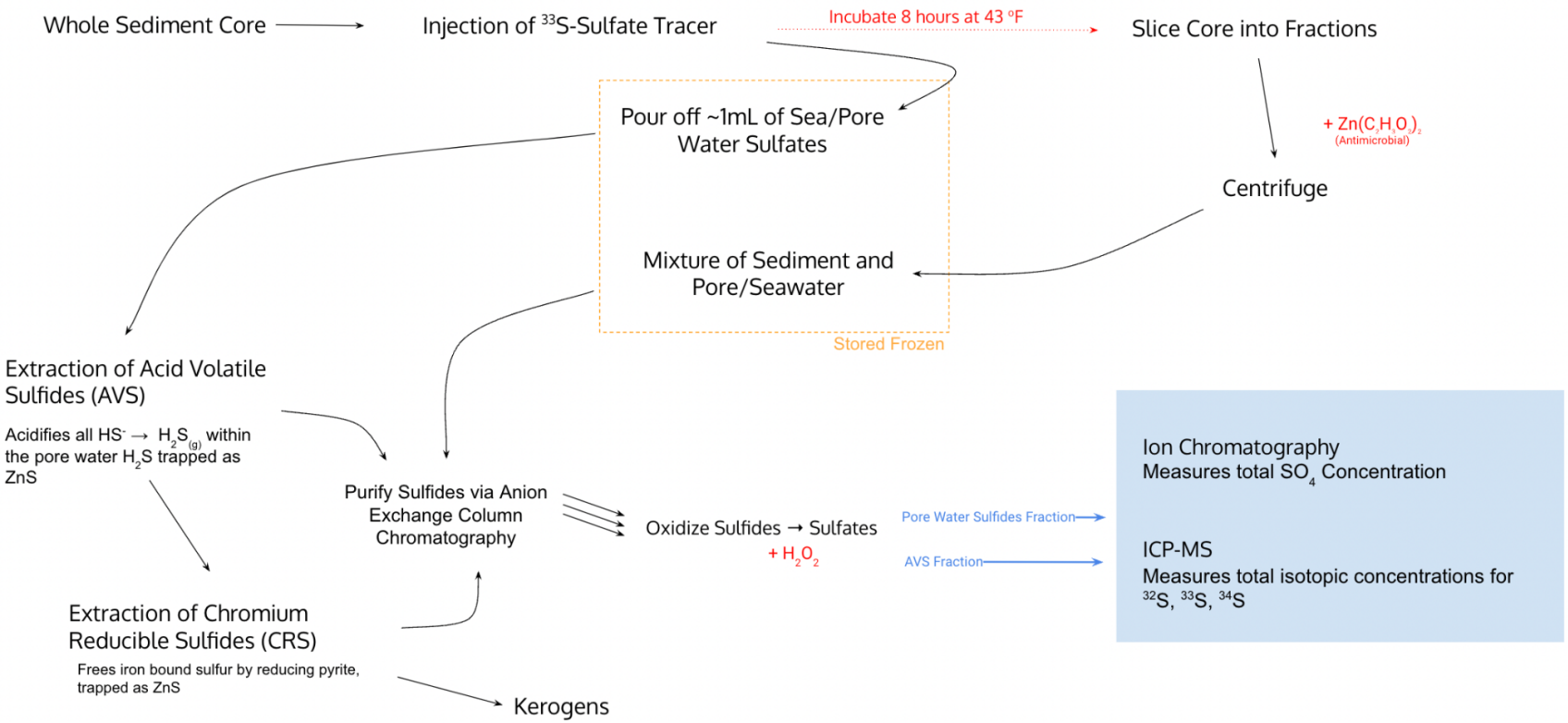

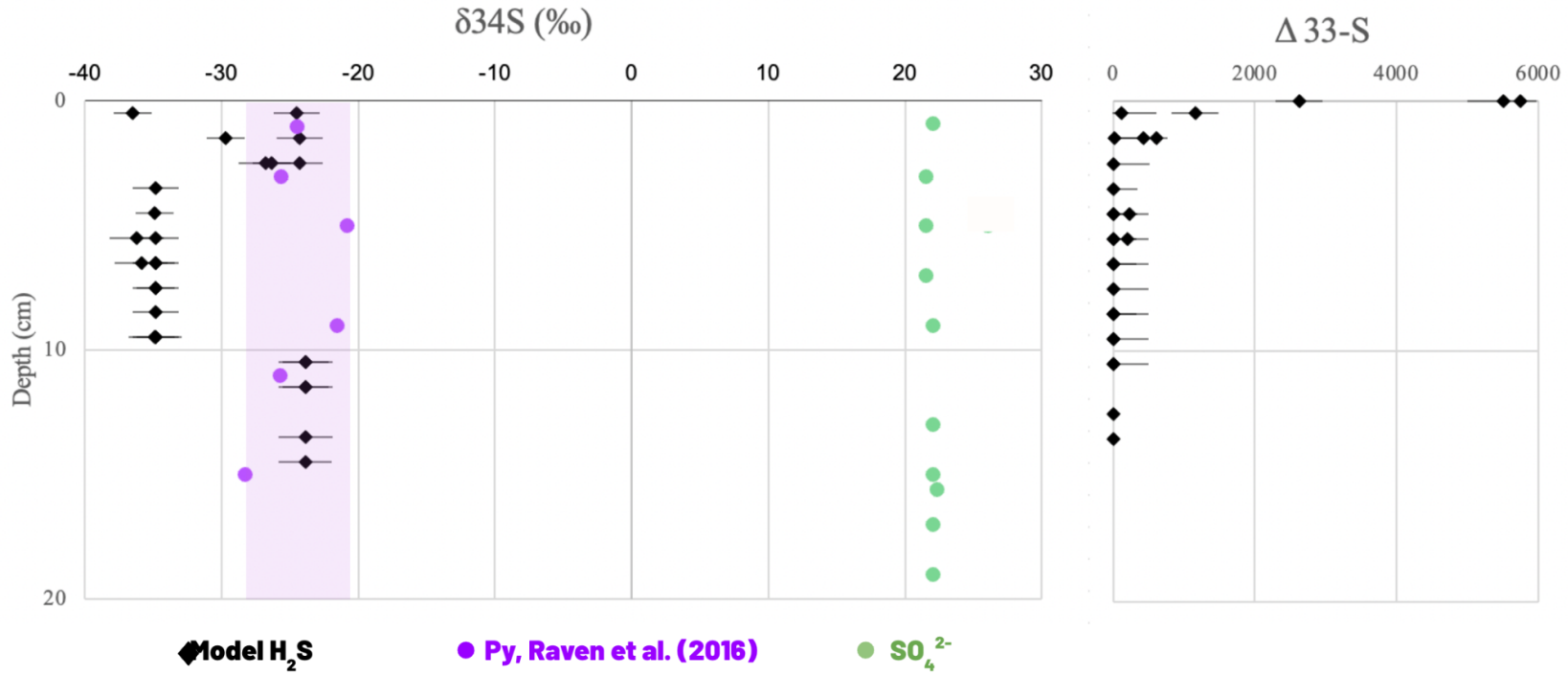

Figure 3.8 Scatter plot of $\delta^{34}S$ values for modeled sulfides, accumulated AVS ($\delta^{34}S$-H_2S), sulfate, and epsilon values published and modeled. LEFT PANEL: All colored dots are $\delta^{34}S$ values measured in Santa Barbara sediments from Raven *et al.* (2016), Brüchert *et al.*, (1995), and Kaplan *et al.* (1963). Blue dots indicate $\delta^{34}S$-SO_4^{2-}, red dots: $\delta^{34}S$-H_2S, green dots: $\delta^{34}S$-Pyrite. Black diamonds are calculated $\delta^{34}S$-H_2S. Estimated $\delta^{34}S$-H_2S were calculated using sediment densities from NDT3A, NDT3C, and SDT1A cores, and estimated % new sulfide from 35 rates measured in parallel cores. Sulfate and epsilon values used in the 33-S model were cited from Raven *et al.* (2016), Brüchert *et al.,* (1995), and Kaplan *et al.* (1963). **RIGHT PANEL:** Epsilon values associated with MSR, gray triangles are values calculated from $\delta^{34}S$ values measured in Santa Barbara sediments from Raven *et al.* (2016), Brüchert *et al.,* (1995), and Kaplan *et al.* (1963), black diamonds are modeled values using the 33-S method.

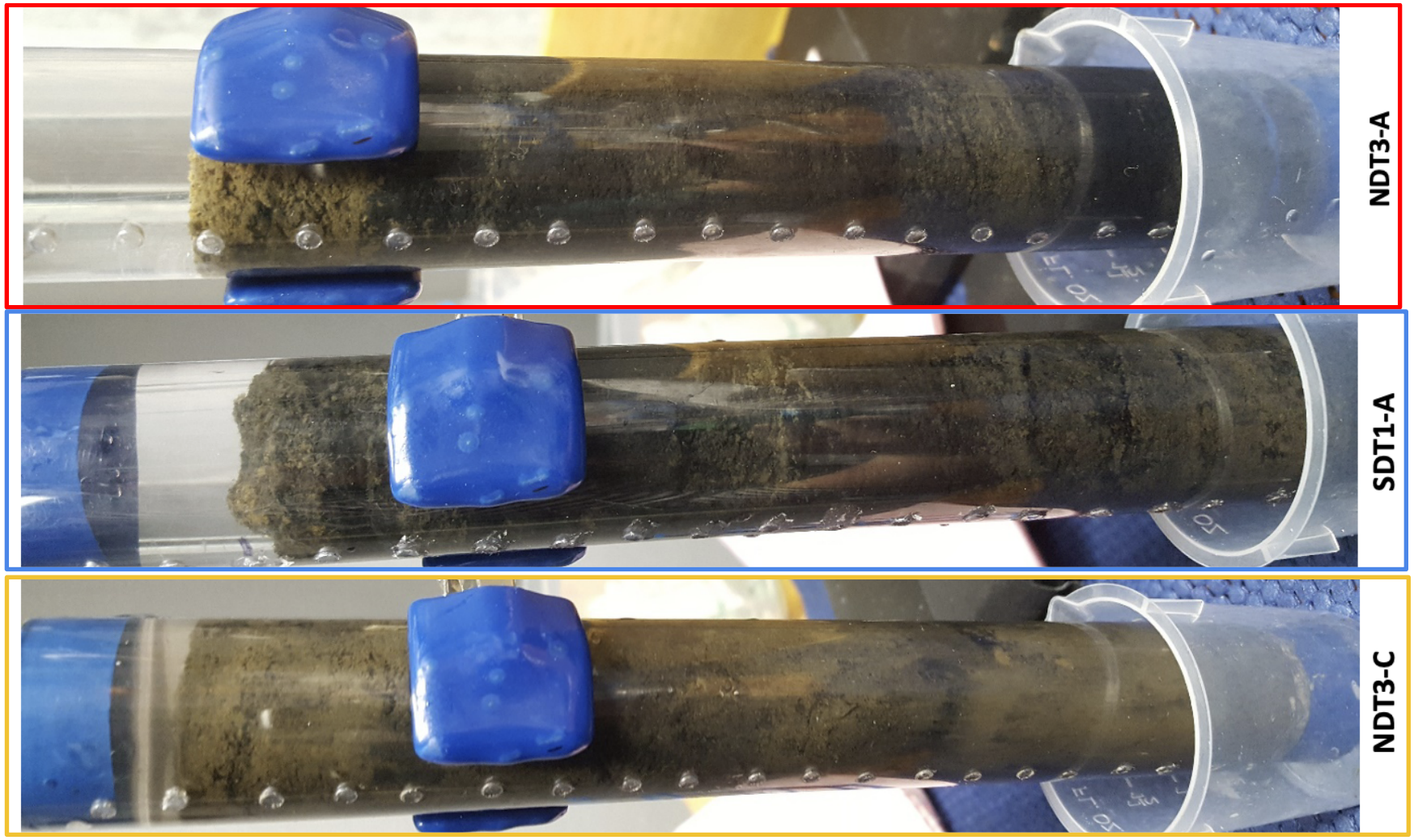

Figure 5.1 Enlarged core images from SBB. NDT3-C, SDT1-A, and NDT3-A f 33-SO_4^{2-} experiment cores rom AT42-19 taken by Molly O'Beirne, Dec 2019